

1 **BrainPalmSeq: A curated RNA-seq database of palmitoylating and de-palmitoylating enzyme**  
2 **expression in the mouse brain**

3

4 **Authors:** Wild, AR<sup>1</sup>; Hogg, PW<sup>1</sup>; Flibotte, S<sup>2</sup>; Nasseri, G<sup>1</sup>; Hollman, R<sup>1</sup>; Haas, K<sup>1</sup> and Bamji, SX<sup>1</sup>

5

6

7

8 **Affiliations:**

9 1 Department of Cellular and Physiological Sciences, Life Sciences Institute and Djavad Mowafaghian  
10 Centre for Brain Health, University of British Columbia

11 2 Life Sciences Institute Bioinformatics Facility, University of British Columbia

12

13

14

15

16

17

18

19

20

21 **Correspondence:**

22 Shernaz Bamji, Ph.D.

23 Department of Cellular and Physiological Sciences

24 Life Sciences Institute,

25 Djavad Mowafaghian Centre for Brain Health

26 University of British Columbia

27 2350 Health Sciences Mall

28 Vancouver, B.C., V6T 1Z3

29 Off: 604-822-4746

## 30 **Abstract**

31 Protein *S*-palmitoylation is a reversible post translational lipid modification that plays a critical  
32 role in neuronal development and plasticity, while dysregulated *S*-palmitoylation underlies a number of  
33 severe neurological disorders. Dynamic *S*-palmitoylation is regulated by a large family of ZDHHC  
34 palmitoylating enzymes, their accessory proteins, and a small number of known de-palmitoylating  
35 enzymes. Here, we curated and analyzed expression data for the proteins that mediate *S*-palmitoylation  
36 from publicly available RNAseq datasets, providing a comprehensive overview of their distribution in the  
37 mouse nervous system. We developed a web-tool that enables interactive visualization of the expression  
38 patterns for these proteins in the nervous system (<http://brainpalmseq.med.ubc.ca/>), and explored this  
39 resource to find region and cell-type specific expression patterns that give insight into the function of  
40 palmitoylating and de-palmitoylating enzymes in the brain and neurological disorders. We found  
41 coordinated expression of ZDHHC enzymes with their accessory proteins, de-palmitoylating enzymes and  
42 other brain-expressed genes that included an enrichment of *S*-palmitoylation substrates. Finally, we  
43 utilized ZDHHC expression patterns to predict and validate palmitoylating enzyme-substrate interactions.

44

## 45 **Introduction**

46 Protein *S*-palmitoylation is a post-translational lipid modification that mediates dynamic changes  
47 in protein stability, function, and membrane localization. *S*-palmitoylation is defined as the reversible  
48 formation of a cysteine residue thioester bond with the fatty acid palmitate, and is the most prevalent  
49 post translational lipid modification in the brain. Dynamic changes in *S*-palmitoylation are critical for  
50 neuronal development and synaptic plasticity (Fukata et al., 2013; Fukata and Fukata, 2010; Globa and  
51 Bamji, 2017; Matt et al., 2019), oligodendrocyte differentiation and myelination (Ma et al., 2021;  
52 Schneider et al., 2005), and astrocyte proliferation (Yuan et al., 2021). Furthermore, numerous  
53 neurological and psychiatric diseases have now been attributed to mutations in the genes encoding  
54 palmitoylating and de-palmitoylating enzymes, including schizophrenia, intellectual disability and CLN1  
55 disease (Mukai et al., 2004; Nita et al., 2016; Raymond et al., 2007), underscoring the importance of  
56 properly regulated *S*-palmitoylation in normal brain function.

57 *S*-Palmitoylation is mediated by a family of ZDHHC enzymes that share a consensus 'asp-his-his-  
58 cys' catalytic domain. These enzymes are structurally heterogeneous multi-pass transmembrane proteins  
59 that localize to a variety of intracellular compartments, including the golgi, endoplasmic reticulum (ER),  
60 recycling endosomes and the plasma membrane (Globa and Bamji, 2017). The ZDHHC enzymes are known

61 to be associated with accessory proteins that regulate their stability, activity, and trafficking (Salaun et al.,  
62 2020). Several de-palmitoylating enzymes have also been identified that act as the ‘erasers’ of S-  
63 palmitoylation, and are divided into three classes: the acyl-protein thioesterases that shuttle between the  
64 golgi and cytosol (APTs; Vartak et al., 2014), the predominantly lysosomal palmitoyl-protein thioesterases  
65 (PPTs; Koster and Yoshii, 2019) and the more recently discovered  $\alpha/\beta$  hydrolase domain-containing 17  
66 proteins (ABHD17; Lin and Conibear, 2015). Unlike other post-translational modifications, palmitoylation  
67 lacks a consensus substrate amino sequence, and the mechanisms that govern ZDHHC enzyme-substrate  
68 interactions are controversial, with contrasting reports of substrate interactions being both promiscuous  
69 and specific (Malgapo and Linder, 2021). Currently these interactions are thought to be governed by the  
70 subcellular targeting of ZDHHCs enzymes and the presence of protein-protein interacting motifs within  
71 the ZDHHC N- and C-termini, which are highly diverse among the ZDHHC enzymes (Rana et al., 2018).  
72 Differential gene expression can also have a profound influence on protein interactions, and may play a  
73 role in the coordination of S-palmitoylation in the brain. However, a detailed overview and analysis of the  
74 precise cellular and regional expression patterns of the palmitoylating and de-palmitoylating enzymes has  
75 not yet been described, and as such little is known about how this expression is coordinated in the nervous  
76 system.

77         Recent advances in single-cell RNA sequencing (scRNAseq) techniques have enabled the  
78 classification of neuronal and non-neuronal cell types in unprecedented detail, providing a better  
79 understanding of cellular diversity and function in the nervous system, while also providing a means to  
80 study the expression patterns of individual genes across an ever-expanding range of brain regions and  
81 cellular classifications. Here, we capitalized on the recent surge in RNAseq publications characterizing  
82 regional and cellular transcriptomics of the mouse nervous system. We curated and analyzed expression  
83 data from a number of publicly available RNAseq mouse datasets to generate a detailed analysis of the  
84 expression patterns of the genes associated with S-palmitoylation in the mouse brain. Furthermore, we  
85 present an interactive web tool to allow user-driven interrogation of the expression patterns of  
86 palmitoylating and de-palmitoylating enzymes from numerous collated studies across a variety of brain  
87 regions and cell-types (<http://brainpalmseq.med.ubc.ca/>). We demonstrate the utility of this resource by  
88 detailing the considerable cell type and regional heterogeneity in expression patterns of these enzyme  
89 families and their accessory proteins, revealing numerous cell type enrichments and co-expression  
90 patterns that allowed us to generate and test hypotheses about palmitoylating enzyme-substrate  
91 interactions.

## 92 Results

### 93 **BrainPalmSeq: an interactive database to search palmitoylating and depalmitoylating enzyme** 94 **expression in the mouse brain**

95 The recent development of scRNAseq has revolutionized our understanding of the complex  
96 transcriptional diversity of neuronal and non-neuronal cell types in the brain. We found however, there  
97 were several barriers to the easy access for much of this data, with no single resource available to evaluate  
98 multi-study expression data. Data can also be difficult to access when studies are not accompanied by an  
99 interactive online web viewer, while datasets that do have a web viewer employ diverse interfaces that  
100 are often complex, particularly for large scRNAseq datasets. Furthermore, the differing study specific  
101 analysis pipelines, as well as the variety of data presentation formats in web viewers including heatmaps,  
102 bar charts, tables or t-SNE plots can make datasets difficult for non-bioinformaticians to interpret and  
103 compare. In order to remove these barriers and provide easy access to expression data for the proteins  
104 that regulate S-palmitoylation in the brain, we created 'BrainPalmSeq', an easy-to-use web platform  
105 allowing user driven interrogation of compiled multi-study expression data at cellular resolution through  
106 simple interactive heatmaps that are populated according to user selected brain regions, cell-types or  
107 genes of interest (<http://brainpalmseq.med.ubc.ca/>).

108 To create BrainPalmSeq we first curated three large datasets from whole-brain scRNAseq studies  
109 to provide high resolution expression data covering hundreds of cell types at a variety of developmental  
110 ages, acquired through selection-free cell sampling (Rosenberg et al., 2018; Saunders et al., 2018; Zeisel  
111 et al., 2018). As scRNAseq has several caveats including low sensitivity and high frequency of dropout  
112 events leading to incomplete detection of expressed genes (Haque et al., 2017), we complement these  
113 datasets where possible with curation of several bulk and pooled-cell RNAseq studies that used  
114 population-level ensemble measurements from whole-brain and region-specific studies. We further  
115 include selected studies for the major glial cell types and data from the most comprehensive neuron  
116 specific study performed to date by the Allen Institute (Table S1). Together, the datasets curated in  
117 BrainPalmSeq cover all major regions of the mouse nervous system at a variety of sequencing resolutions.

118 Expression data were extracted from selected studies for the 24 mouse ZDHHC genes (*Zdhhc1-*  
119 *Zdhhc25*, while *Zdhhc10* is omitted), as well as the best characterized de-palmitoylating enzymes (*Ppt1*,  
120 *Lypla1*, *Lypla2*, *Abhd17a*, *Abhd17b* and *Abhd17c*) and ZDHHC accessory proteins (*Golga7*, *Golga7b* and  
121 *Selk*). Where possible, data were processed from the raw transcripts or unique molecular identifier (UMI)  
122 counts using the same normalization protocol to allow for more consistent evaluation of differences in

123 gene expression within datasets. We sampled from RNAseq datasets that used a diverse range of sample  
124 collection, processing and analysis techniques, therefore the relative expression patterns of selected  
125 genes can be directly visualized within datasets, and users can then validate their observations across  
126 complimentary whole brain or region/cell-type specific datasets included in BrainPalmSeq. Dropdown  
127 menus allow for selection of individual ZDHHC genes or brain regions within each dataset, while the hover  
128 tool reveals metadata for each cell-type, including neurotransmitter designations and marker genes. We  
129 provide download links to all expression data including cell-type metadata so that users can replot gene  
130 expression profiles in their preferred format. To demonstrate the utility of this resource, we performed a  
131 detailed exploration of selected datasets from BrainPalmSeq, revealing how expression patterns can give  
132 insights into the function of the palmitoylating and de-palmitoylating enzymes in the mouse brain.

### 133 **ZDHHC expression in the nervous system shows regional and cell-type specific patterning**

134 We began by exploring BrainPalmSeq data curated from the ‘MouseBrain’ dataset, which provides  
135 the broadest overview of expression patterns in the nervous system (Zeisel et al., 2018). This scRNAseq  
136 study sampled multiple dissected regions from the adolescent (mean age ~P25) mouse central and  
137 peripheral nervous systems (CNS and PNS), identifying 265 transcriptomically unique cell-types (referred  
138 to herein as metacells) for which we plotted re-normalized ZDHHC expression values, according to the  
139 hierarchical cell-type clustering established by the original study (Figure 1A). While ZDHHC expression was  
140 detected in all regions of the nervous system, expression of the 24 ZDHHC genes was highly variable across  
141 metacell types and clusters. We measured the mean ZDHHC expression within each cluster to gain insight  
142 into which cell-types in the nervous system have the greatest overall expression of palmitoylating  
143 enzymes. The heatmap rows and columns were ranked (sorted by averages descending) to determine  
144 which cell-types had the highest expression of ZDHHCs, and which ZDHHCs were most abundantly  
145 expressed across cell-types (Figure 1B). Mean ZDHHC expression was particularly high in neurons of the  
146 PNS, along with cholinergic/monoaminergic and hindbrain neurons of the CNS. Of the non-neuronal  
147 metacell clusters, oligodendrocytes had the highest ZDHHC expression, while other glial cell-types appear  
148 at the lower end of the ranking (Figure 1B). *Zdhhc20* was the most abundantly expressed ZDHHC, with the  
149 highest mean expression across all cell-type clusters, followed by *Zdhhc2*, *Zdhhc17*, *Zdhhc3* and *Zdhhc21*,  
150 while expression of *Zdhhc11*, *Zdhhc19* and *Zdhhc25* was negligible. We next clustered neuronal metacells  
151 of the PNS and CNS according to the neurotransmitter combinations, revealing the highest mean ZDHHC  
152 expression was observed in neurons that utilized acetylcholine and nitric oxide as co-neurotransmitters,  
153 with cholinergic neurons featuring near the top of the list in several neurotransmitter combinations  
154 (Figure 1C). Monoaminergic neurons utilizing noradrenaline and serotonin also generally ranked high in

155 the list, consistent with the data in Figure 1B that ranked cholinergic and monoaminergic neurons as the  
156 metacell cluster with the highest CNS ZDHHC expression overall, indicating a higher propensity for these  
157 cell-types to utilize S-palmitoylation as a post-translational mechanism to modify cellular signaling. We  
158 performed comparative analysis of ZDHHC expression on another large-scale scRNAseq study of the  
159 mouse brain that sampled a variety of cortical and subcortical structures of the adult mouse (P60-P70)  
160 (Saunders et al., 2018; 'DropViz'; Figure S1A). We found expression patterns and enrichments to be similar  
161 across these two independent, large scale scRNAseq studies, supporting the general trends observed with  
162 the MouseBrain dataset.

163 To gain insight into the networks of ZDHHC enzymes that might work together to coordinate S-  
164 palmitoylation in different cell types we performed co-expression analysis (Spearman correlation)  
165 between ZDHHC genes across all 265 metacell types in the MouseBrain dataset (Figure 1D; Table S2).  
166 Neuron enriched *Zdhhc3*, *Zdhhc8*, *Zdhhc17* and *Zdhhc21* formed the strongest network of co-expression  
167 associations, while glial cell enriched *Zdhhc2*, *Zdhhc9* and *Zdhhc20* formed less robust correlations with  
168 other ZDHHCs. Weaker correlations were observed across the 565 cell-types in the DropViz dataset, which  
169 may reflect the absence of the PNS neurons and glia in this study (Figure S1D; Table S2).

170 In order to create a list of potential substrates for the ZDHHCs in the mouse nervous system, we  
171 expanded our co-expression analysis to include all expressed genes from the 'MouseBrain' dataset that  
172 had significant correlation ( $R > 0.7$ ) with one or more ZDHHC. We identified 914 genes that were  
173 significantly correlated with DHHCs. This list was cross-referenced with the mouse SwissPalm database of  
174 S-palmitoylated substrates identified in at least one palmitoyl-proteome or experimentally validated  
175 (SwissPalm annotated; Blanc et al., 2015, 2019). We found that genes that showed correlated expression  
176 with a ZDHHC were significantly enriched with S-palmitoylation substrates, indicating that ZDHHCs are  
177 more likely to be co-expressed with their S-palmitoylation substrates in the brain (Figure 1E; Table S3).  
178 Co-expression analysis of the 'DropViz' dataset revealed a similar enrichment of S-palmitoylation  
179 substrates co-expressed with ZDHHCs (Figure S1E; Table S4), supporting the notion of ZDHHC enzyme-  
180 substrate co-expression. PANTHER GO analysis of the 'MouseBrain' curated ZDHHC co-expressed S-  
181 palmitoylation substrates revealed several significant enrichments in GO terms for biological processes  
182 related to protein localization (Figure 1F), as well as enrichments for cellular components that included  
183 synapses, membrane-bounded organelles, endomembranes and vesicles (Figure S2B). These findings are  
184 consistent with the known role of S-palmitoylation in regulating protein localization and signaling  
185 complexes at cellular membranes.

## 186 **Heterogeneity in ZDHHC expression within excitatory neurons of the dorsal hippocampus**

187           The hippocampus is a heavily studied brain region that is critical for learning and memory (Bird  
188 and Burgess, 2008). A recent pooled-cell RNAseq study of excitatory neurons in the hippocampus revealed  
189 extensive regional variability in gene expression profiles of the hippocampal tri-synaptic loop  
190 (hipposeq.janelia.org; Cembrowski et al., 2016). In order to clearly visualize if ZDHHC expression also  
191 varied in these different cell populations, we projected log transformed expression heatmaps generated  
192 in BrainPalmSeq for the ‘hipposeq’ dorsal-ventral excitatory neuron dataset on to anatomical maps of the  
193 dorsal hippocampus (Figure 2A). We observed considerable heterogeneity in the regional expression  
194 patterns of the ZDHHCs. Hierarchical clustering analysis revealed that the ZDHHCs could be grouped into  
195 those that showed similar expression in all regions, those that were dentate gyrus granule cell (DG)  
196 enriched, DG depleted or CA1/CA2 enriched (Figure 3B). We generated comparative heatmaps for several  
197 scRNAseq studies curated in BrainPalmSeq that also quantified the hippocampal excitatory neuron  
198 transcriptome and found similar cross-study expression patterns for many of the ZDHHCs (Figure S3A).  
199 Furthermore, *in situ* hybridization data from the Allen Institute showed a high degree of overlap with the  
200 ‘hipposeq’ derived ZDHHC expression patterns, supporting the replicability of the expression patterns  
201 observed in the ‘hipposeq’ dataset (Figure S3B; Table S5).

202           We next sought to utilize the ‘hipposeq’ dataset to determine if there might be regional  
203 differences in the expression of S-palmitoylation substrates in excitatory neurons of the dorsal  
204 hippocampus, which may be potential substrates for regionally enriched ZDHHC enzymes. To investigate  
205 the regionally-enriched predicted hippocampal palmitoylome, we utilized the enrichment analysis tools  
206 built in to hipposeq.janelia.org (see materials and methods). Neurons in each hippocampal sub-region  
207 expressed unique S-palmitoylation substrates that were related to highly divergent functions. We found  
208 for CA1 neurons, which have highest expression of *Zdhhc2*, *Zdhhc17*, *Zdhhc23* and *Zdhhc9* (Figure 3C), the  
209 CA1 enriched predicted palmitoylome (Figure 3D; Table S6) generated KEGG pathways related to ‘Calcium  
210 signaling’, ‘Glutamatergic synapse’ and ‘Long term potentiation’, supporting the known role S-  
211 palmitoylation plays in CA1 hippocampal synaptic plasticity (Figure 3E; Ji and Skup, 2021; Matt et al.,  
212 2019). The CA1 predicted palmitoylome was composed of around 46 % synaptic proteins (SynGO  
213 annotated), with SynGO ontologies related to ‘synaptic vesicle exocytosis’ and ‘synapse organization’  
214 (Figure 3F; Koopmans et al., 2019). In contrast, the predicted palmitoylome of DG granule cells which have  
215 the highest expression of *Zdhhc21*, *Zdhhc4*, *Zdhhc24* and *Zdhhc8* (Figure 3G, H) generated KEGG pathways  
216 related to ‘Ribosome’, ‘Cholinergic synapse’ and ‘Parkinson’s disease’ (Figure 3I). The DG predicted-  
217 palmitoylome was composed of 29 % synaptic proteins (SynGO annotated), with SynGO ontologies related

218 to ‘protein translation at presynapse’ and ‘protein translation at postsynapse’, revealing a potential role  
219 for palmitoylating enzymes in regulating translation in this cell-type that has not yet been studied (Figure  
220 3J). Together, we have described patterns of restricted expression of ZDHHC enzymes and S-  
221 palmitoylation substrates in the dorsal mouse hippocampus, and generated both broad and regionally-  
222 enriched predicted-palmitoylomes that give insight into the role of S-palmitoylation in neuronal function  
223 in each of these hippocampal sub-regions.

#### 224 **Neocortical ZDHHC expression is partially segregated across cortical layers and neuronal subclasses**

225 We next examined scRNAseq datasets curated in BrainPalmSeq from the cortex, beginning with a  
226 study of the primary somatosensory cortex (SSp; Zeisel et al., 2015). We projected heatmaps of pyramidal  
227 excitatory neuron ZDHHC expression generated in BrainPalmSeq onto cortical layer diagrams of SSp, again  
228 revealing anatomically heterogeneous excitatory neuron expression patterns of several of the ZDHHC  
229 transcripts. Clustering primarily grouped the enzymes according to expression levels, with *Zdhhc21*,  
230 *Zdhhc17* and *Zdhhc8* having the highest relative expression (Figure 3B). *Zdhhc2*, *Zdhhc3* and *Zdhhc20*  
231 expression was also high, with the remainder of the ZDHHCs having moderate to low expression. We  
232 compared these expression patterns with other datasets curated in BrainPalmSeq (Figure S4A), which  
233 revealed many consistent patterns of expression maintained across several independent studies. For  
234 example, multiple studies reported high expression of *Zdhhc8* in cortical Layer 2/3, enrichment of *Zdhhc2*  
235 in Layer 4 and elevated expression of *Zdhhc21* in all layers, particularly in Layer 5. *Zdhhc3* and *Zdhhc20*  
236 were also broadly expressed in all cortical layers across studies. Similar patterns were seen in the SSp  
237 region from available in situ hybridization studies from Allen Brain Institute (Figure S3B).

238 We examined expression patterns of the ZDHHC enzymes from one of the largest neuronal  
239 scRNAseq studies from the isocortex performed by the Allen Brain Institute, which identified 236  
240 glutamatergic and 117 GABAergic distinct neuron metacell types (Yao et al., 2021). We averaged ZDHHC  
241 expression data downloaded from BrainPalmSeq for the major metacell clusters from all regions of the  
242 isocortex, according to their anatomical location and/or axon projection and plotted ranked heatmaps  
243 (Figure 3C,D). We again found that *Zdhhc20* was the ZDHHC transcript with the highest expression, with  
244 broad expression across the majority of glutamatergic and GABAergic cell-types. Elevated expression of  
245 *Zdhhc14* was found in both glutamatergic and GABAergic neurons, which was moderately expressed in  
246 other studies of the brain and cortex discussed previously. Numerous subtypes of projection neurons  
247 featured at the top of the ranking including pyramidal tract (PT) projecting neurons found in layer 5 of the  
248 cortex, that have extensive dendritic branching and long-range axonal projections to the spinal cord,



249 brainstem and midbrain, as well as the ipsilateral cortex, striatum and thalamus. Other neuron subtypes  
250 with high ZDHHC expression included a number of intratelencephalic (IT) projecting neuron classes,  
251 including those from Layer 4/5 of the temporal/perirhinal/ectorhinal/entorhinal cortices, Car3 expressing  
252 Layer 6 neurons, Layer 6b neurons, and Cortex IT projecting neurons from all cortical layers (Harris and  
253 Shepherd, 2015; Yao et al., 2021). GABAergic neurons of the isocortex also showed elevated expression  
254 of the common neuronal ZDHHCs including *Zdhhc2*, *Zdhhc3*, *Zdhhc14*, *Zdhhc17*, *Zdhhc20* and *Zdhhc21*.  
255 The highest mean ranked expression was observed in the recently categorized Sncg neurons that  
256 correspond to *Vip*<sup>+</sup>/*Cck*<sup>+</sup> multipolar or basket cells (Tasic et al., 2018), and lowest expression was observed  
257 in *Vip* subclass of interneurons.

258 Together, our observations reveal that the complex transcriptional diversity of neurons that has  
259 recently been revealed by RNA sequencing also includes heterogeneity in the expression of the ZDHHC  
260 enzymes that mediate palmitoylation. These expression patterns are likely to influence enzyme-substrate  
261 interactions along with the function of S-palmitoylation substrates, and as such have an influence over  
262 neuronal development, function and synaptic plasticity.

### 263 **De-palmitoylating enzyme and ZDHHC accessory protein expression in the nervous system shows** 264 **regional and cell-type specific patterning**

265 Dynamic turnover of protein S-palmitoylation is mediated by the activity of de-palmitoylating  
266 enzymes, which determine the half-life of S-palmitoylation on a target protein. These include acyl-protein  
267 thioesterases 1 and 2 (APT1, APT2; encoded by *Lypla1*, *Lypla2*), palmitoyl-protein thioesterase 1 (PPT1)  
268 and the more recently identified  $\alpha/\beta$  hydrolase domain-containing 17 proteins (ABHD17A, ABHD17B and  
269 ABHD17C). Compared with the ZDHHC enzymes, relatively less is known about the substrates, sub-cellular  
270 localization and brain expression patterns of this family of enzymes. We next explored BrainPalmSeq to  
271 determine which cell-types/brain regions show the highest expression of de-palmitoylating enzymes.

272 We first examined expression heatmaps for the known de-palmitoylating enzymes across the 265  
273 cell-types identified in the 'MouseBrain' dataset (Figure 4A) and the cell-type averages for the 565 cell-  
274 types from the 'DropViz' dataset (Figure S4A). *Ppt1* and *Abhd17a* were the enzymes with the broadest  
275 expression across all cell-types, with *Ppt1* expression being notably elevated in neurons of the hindbrain  
276 and immune cells, and *Abhd17a* being elevated in hindbrain neurons, sensory neurons, oligodendrocytes  
277 and epithelial cells. Ranked expression (sorted by averages descending) of de-palmitoylating enzymes in  
278 the 'MouseBrain' (Figure 4B) and 'DropViz' (Figure 4C) ranked oligodendrocyte lineage cells among the  
279 cell-types with the highest expression of de-palmitoylating enzymes overall, primarily due to elevated

280 expression of *Abhd17b*, mirroring oligodendrocyte enrichment of ZDHHC enzyme expression and again  
281 indicating that dynamic regulation of S-palmitoylation may be particularly important in this cell type.  
282 *Lypla2* expression was greater than *Lypla1* overall in the brain, with *Lypla2* expression being highest in  
283 neurons and ependymal cells. *Abhd17c* had the lowest brain expression of all the de-palmitoylating  
284 enzymes studied. Correlation analysis between the ZDHHCs and de-palmitoylating enzymes revealed  
285 numerous instances of co-expression with almost every ZDHHC (Figure 4D), revealing potential  
286 cooperative pairs of palmitoylating and de-palmitoylating enzymes in the nervous system.

287         Although the ZDHHC enzymes are thought to have the ability to act autonomously, several  
288 accessory proteins have been discovered that can regulate ZDHHC stability, localization and catalytic  
289 activity (Salaun et al., 2020). These include GOLGA7 (GCP16), which can bind to ZDHHC9 enhancing both  
290 protein stability and increasing enzymatic activity by stabilizing the ZDHHC9 auto-palmitoylated  
291 intermediate that is formed prior to palmitate transfer to the substrate protein (Mitchell et al., 2014;  
292 Swarthout et al., 2005). Both GOLGA7 and related isoform GOLGA7B are also able to interact with  
293 ZDHHC5, with the latter having an influence on ZDHHC5 plasma membrane localization (Woodley and  
294 Collins, 2019). Finally, SELK (SELENOK; Selenoprotein K) is an ER localized protein that was found to  
295 interact with ZDHHC6, stabilize the auto-palmitoylated intermediate and increase palmitoylation of  
296 substrate proteins including the IP<sub>3</sub> receptor (Fredericks et al., 2017, 2014).

297         Widespread expression of *Selk* was observed across all cell-types, with expression being  
298 considerably higher than any of the ZDHHCs, de-palmitoylating enzymes or other accessory proteins  
299 (Figure 4A, S4A). This is consistent with the known functions of SELK in the ER associated protein  
300 degradation pathway and regulation of ER calcium flux (Pitts and Hoffmann, 2018). *Golga7b* expression  
301 was widespread across neuronal subtypes but barely detected in glial cells (Figure 4A, S4A). Accordingly,  
302 *Golga7b* expression was also strongly correlated with several of the ZDHHCs that were most highly  
303 expressed in neurons, including *Zdhhc3*, *Zdhhc8*, *Zdhhc17* and *Zdhhc21* (Figure 4D). In contrast, *Golga7*  
304 was enriched in glial cells, particularly in oligodendrocytes, similar to ZDHHC9 for which GOLGA7 is a key  
305 accessory protein (Figure 4A, S4A). GOLGA7 and GOLGA7B share 61% amino acid similarity, but their  
306 expression was either not correlated or negatively correlated (Table S2), indicating that the ZDHHC  
307 association of each of these proteins may be regulated in part by differential expression.

### 308 **Loss of function mutations in palmitoylating and de-palmitoylating**

309         Impaired regulation of S-palmitoylation has been implicated in numerous neurological disorders,  
310 many of which are due to loss of function (LOF) mutations in palmitoylating and de-palmitoylating

311 enzymes (Cho and Park, 2016; Matt et al., 2019). We next sought to determine if the regional and cell  
312 type expression data available in BrainPalmSeq could reveal insights into the pathogenesis of disorders  
313 caused by LOF mutations in palmitoylating and de-palmitoylating enzymes. As many of these diseases  
314 have a neurodevelopmental origin, we examined whole brain datasets curated in BrainPalmSeq from the  
315 neonatal (Rosenberg et al., 2018), adolescent (Zeisel et al., 2018) and adult (Sjöstedt et al., 2020) mouse  
316 brain.

317 A single nucleotide polymorphism (SNP) in the *ZDHHC8* gene has been implicated in increased  
318 susceptibility to schizophrenia (Chen et al., 2004; Mukai et al., 2004), while hemizygous microdeletion in  
319 the chromosomal locus 22q11, which encodes a number of genes including *ZDHHC8*, is one of the highest  
320 known genetic risk factors to developing schizophrenia (Figure 5A; Karayiorgou et al., 2010). To assess the  
321 developmental expression of *Zdhhc8*, we averaged expression within broadly defined cell-type clusters  
322 that could be applied to both the Rosenberg and Zeisel scRNAseq datasets (Figure 5A, B; Table S7). *Zdhhc8*  
323 expression was highest in neurons of the cortex and hippocampus, followed by neurons of the mid- and  
324 hindbrain at both developmental ages. To explore regional expression in the adult mouse brain, we  
325 projected BrainPalmSeq generated heatmaps expression data from the ‘Protein Atlas’ mouse whole brain  
326 dataset (bulk RNAseq from 13 brain regions) onto anatomical maps of the mouse brain, again revealing  
327 highest expression of *Zdhhc8* in the cortex, followed by the hippocampus and basal ganglia (Figure 5C;  
328 Sjöstedt et al., 2020). *Zdhhc8* expression was particularly enriched in Layer 2/3 of the neonatal (not shown)  
329 and adult mouse cortex (Figure S3B), which is the cortical layer with the most pronounced morphological  
330 deficits in patients with Schizophrenia (Glantz and Lewis, 2000; Kolluri et al., 2005; Wagstyl et al., 2016).  
331 Together, we found *Zdhhc8* expression patterns in the mouse brain that are established early in postnatal  
332 development and maintained into adulthood, that also overlay with many brain regions and cell types  
333 that are known to be severely affected in patients with schizophrenia. These observations support a model  
334 in which LOF *ZDHHC8* mutations may elicit many of the symptoms of schizophrenia by disrupting S-  
335 palmitoylation and normal neuronal development in these brain regions.

336 Mutations in the *ZDHHC9* gene, which is located on the X chromosome, have been identified in  
337 ~2% of X-linked intellectual disability (ID) patients (Raymond et al., 2007; Tzschach et al., 2015).  
338 Neuroanatomical abnormalities reported in patients with *ZDHHC9* mutations include decreased cortical,  
339 thalamic and striatal volume, and widespread white matter abnormalities with prominent hypoplasia  
340 (under-development) of the corpus callosum (Baker et al., 2015; Bathelt et al., 2016). Disrupted white  
341 matter integrity is thought to underlie deficits in global and local brain connectivity in patients with

342 *ZDHHC9* mutations (Bathelt et al., 2017). *Zdhhc9* knock-out mice also develop similar pathological  
343 changes, including decreased volume of the corpus callosum (Kouskou et al., 2018). We observed  
344 considerable cell-type enrichment of *Zdhhc9* in oligodendrocytes across studies and developmental ages  
345 (Figure 5D, E), accompanied by moderate neuronal expression of *Zdhhc9* relative to other ZDHHCs across  
346 several brain regions including the hippocampus and cortex (Figure 2A, 3A, 5D, E), consistent with the  
347 known function of ZDHHC9 in regulating neuronal development (Shimell et al., 2019). Regionally, we  
348 found *Zdhhc9* expression in adult mice to be highly enriched in the corpus callosum, the largest white  
349 matter tract in the brain (Figure 5F). As myelin production by oligodendrocytes is critical for maintaining  
350 white matter integrity, these observations indicate that disrupting S-palmitoylation in oligodendrocytes  
351 may underlie the white matter pathology and decreased connectivity observed in patients with X-linked  
352 ID and *ZDHHC9* mutations.

353         Infantile neuronal ceroid lipofuscinosis (INCL or CLN1 disease) is a severe neurological disorder  
354 caused by LOF mutations in the *PPT1* gene that presents in the first 6 - 12 months of life and is  
355 characterized by rapid developmental regression, blindness and seizures, with continual deterioration  
356 until death in early childhood (Nita et al., 2016). While PPT1 is thought to primarily localize to lysosomes  
357 with an essential role in lysosomal degradation of S-palmitoylated proteins (Lu et al., 1996), PPT1 also has  
358 a synapse-specific function in regulating synaptic vesicle cycling and synaptic transmission (Koster and  
359 Yoshii, 2019). We found that neuronal *Ppt1* expression was high in postnatal neurons of the spinal cord,  
360 olfactory bulb and mid/hindbrain, while microglia were the highest expressing non-neuronal cell type at  
361 both postnatal ages (Figure 5G, H). Neurodegeneration has been detected in the spinal cord prior to their  
362 onset within the brain in *Ppt1* knock-out mice, accompanied by extensive glial cell activation including  
363 microgliosis, which is a pathological hallmark of CLN1 disease (Shyng et al., 2017). Mid-/hindbrain neurons  
364 also had high expression of *Ppt1*, consistent with reports that *Ppt1* knock-out mice show earliest signs of  
365 brain pathology in the thalamus (Kielar et al., 2007). Overall, we observed widespread *Ppt1* expression in  
366 almost every brain region in adult mice, consistent with the sweeping neurological deficits associated with  
367 CLN1 disease (Figure 5I). Together, these observations reveal how the loss of *Ppt1* in cell types with high  
368 *Ppt1* expression may lead to cell death/dysfunction in the early stages of CLN1 disease.

### 369 **ZDHHC cell type enrichments can be used to predict and validate ZDHHC substrates**

370         We next tested if ZDHHC expression patterns identified from BrainPalmSeq could be used to  
371 predict and validate S-palmitoylation substrates for regionally enriched ZDHHCs. We focused on *Zdhhc9*,  
372 which showed a consistent cell-type enrichment in oligodendrocytes across multiple studies in

373 BrainPalmSeq, while LOF mutations in *ZDHHC9* are known to result in decreased white matter integrity in  
374 the brain (Raymond et al., 2007). Examination of the Marques et al oligodendrocyte-specific scRNAseq  
375 dataset curated in BrainPalmSeq revealed that oligodendrocyte *Zdhhc9* expression increased throughout  
376 maturation, with highest expression in the myelin forming (MFOL) intermediate-maturity subtype  
377 oligodendrocytes, and slightly lower expression maintained in mature oligodendrocytes (MOL; Figure 6A;  
378 Marques et al., 2016).

379 To identify potential substrates for ZDHHC9, we cross-referenced a list of MFOL/MOL enriched  
380 genes identified in the study by Marques et al (Marques et al., 2016) with the SwissPalm database to  
381 identify known palmitoylation substrates in these cell types (Swiss Palm Annotated; Table S8, Figure 6B;  
382 Blanc et al., 2019, 2015). PANTHER analysis of cellular component enrichments for these substrates  
383 revealed the most significant enrichment was for the term ‘myelin sheath’ (30 proteins; Figure 6C, S6). To  
384 determine if any of the myelin sheath associated proteins could be palmitoylated by ZDHHC9, we selected  
385 three proteins (MOBP, PLP1 and CNP) for experimental validation (Figure 6C). We expressed either of  
386 these candidate substrates together with ZDHHC9 and its accessory protein GOLGA7 in HEK293T cells, and  
387 determined the proportion of palmitoylated substrate using an Acyl-Rac palmitoylation assay (Forrester  
388 et al., 2011). In this assay, free cysteine residues of cell lysates were first blocked, followed by cleavage of  
389 the palmitoyl-thioester bond with hydroxylamine, resulting in the exposure of a free sulfhydryl group.  
390 Cleaved lysates were then applied to a sepharose resin to capture palmitoylated proteins containing a  
391 free sulfhydryl group. Un-bound proteins (Unpalm Fraction) were first extracted from the resin mixture,  
392 followed by elution of bound palmitoylated proteins from the resin (Palm Fraction). To assess non-specific  
393 binding of unpalmitoylated protein to the resin, half of the cell lysate was processed without the cleavage  
394 step (NSB control). Co-expression of HA-ZDHHC9 and FLAG-GOLGA7 increased the palmitoylated fraction  
395 of MOBP and PLP1, revealing that these proteins are substrates for ZDHHC9 (Figure 6D, E, G). Conversely,  
396 CNP was not identified as a ZDHHC9 substrate in our assay (Figure 6F, G). These results reveal how the  
397 cell-type enrichments of ZDHHC enzymes identified in this study can be used, along with the lists of  
398 similarly enriched palmitoylation substrates, to guide the identification of enzyme-substrate interactions  
399 that can be further investigated *in vivo*.

400

## 401 **Discussion**

### 402 **BrainPalmSeq as a tool to generate hypotheses about proteins that control S-palmitoylation in the** 403 **brain**

404           We have demonstrated the utility of BrainPalmSeq by providing examples of how this database  
405 can be used to explore detailed region and cell type-specific expression patterns of the known  
406 palmitoylating and de-palmitoylating enzymes, and their accessory proteins. We reveal how these  
407 expression patterns can be used to predict/validate S-palmitoylation substrates and better understand  
408 diseases associated with loss of function mutations in the enzymes that mediate S-palmitoylation. Given  
409 the number of brain regions and cell types incorporated into BrainPalmSeq that were not discussed in the  
410 present study, including the thalamus, hypothalamus, amygdala, striatum and cerebellum, there is rich  
411 potential for users to explore the data and generate hypotheses about the role of these enzymes in the  
412 brain.

### 413 **Insights into the role of S-palmitoylation associated enzymes in brain physiology and pathology**

414           While we found that many of the proteins we studied showed correlated expression across the  
415 entire mouse nervous system, particularly those enriched in neurons including *Zdhhc3*, *Zdhhc8*, *Zdhhc17*  
416 and *Zdhhc21*, expression of these genes was segregated within more narrowly defined neuronal  
417 populations such as the excitatory pyramidal neurons within the hippocampal tri-synaptic loop or layers  
418 of the somatosensory cortex. This is in line with the extensive neuronal transcriptional heterogeneity  
419 identified recently by a number of scRNAseq studies (Saunders et al., 2018; Yao et al., 2021; Zeisel et al.,  
420 2015, 2018). The genes that determine neuronal identity fall under four broad functional categories: those  
421 that control transcriptional programs, membrane conductance, neurotransmission, and synaptic  
422 connectivity (Zeisel et al., 2018). We report also heterogeneity in the neuronal fingerprint of  
423 palmitoylating and de-palmitoylating enzyme expression, which will in turn give rise to differential S-  
424 palmitoylation of neuronal proteins. Future work is needed to determine how these specific ZDHHC  
425 expression patterns are related to dynamic S-palmitoylation in these neuronal sub-types, and how the  
426 elevated expression of certain ZDHHCs can alter neuronal function. Given that S-palmitoylation is key  
427 regulator of neuronal development, and that nearly half of all known synaptic proteins are substrates for  
428 palmitoylation (Sanders et al., 2015), this heterogeneity is likely to be a key mechanism in the fine tuning  
429 of neuronal function and synaptic transmission.

430           Many of the ZDHHCs that we observed with consistently elevated expression across multiple  
431 studies in BrainPalmSeq have already been studied in the context of neuronal signaling, including ZDHHC2,

432 ZDHHC3, ZDHHC8 and ZDHHC17 (Ji and Skup, 2021; Matt et al., 2019). In contrast, ZDHHC20 and ZDHHC21  
433 are relatively understudied in the nervous system, despite our observation that these are two of the most  
434 abundantly expressed ZDHHCs across neuronal cell types, with broad expression of *Zdhhc20* also in glial  
435 cells. A recent study defined a role for ZDHHC21 in the palmitoylation of serotonergic receptor 5-HT1A  
436 and implicated downregulation of ZDHHC21 in the development of major depressive disorder (Gorinski et  
437 al., 2019). Interestingly, both ZDHHC20 and ZDHHC21 have a potential role in the pathogenesis of  
438 Alzheimer's disease, as they can palmitoylate BACE1, Tau and amyloid precursor protein (Cho and Park,  
439 2016). More work is needed to understand the likely important role of these enzymes in the brain.

440 We made several other interesting observations during our examination of BrainPalmSeq that  
441 were not discussed in detail in the present study but we believe warrant further investigation. For  
442 example, the particularly elevated expression of *Zdhhc2* in peripheral sensory neurons may indicate an  
443 important role for palmitoylation in this cell type. Across multiple studies we observed striking enrichment  
444 of *Zdhhc14* in cerebellar Purkinje neurons, a cell type in which S-palmitoylation is known to be important  
445 for long-term depression, although the role of ZDHHC14 in this process has not yet been investigated  
446 (Thomas et al., 2013). *Zdhhc23* was similarly enriched in the CA2 region of the hippocampus, with  
447 comparatively low expression across other cell types. More broadly, the elevated expression of a variety  
448 of palmitoylating enzymes in neurons that utilize acetylcholine or monoamines as neurotransmitters  
449 would suggest an important role for S-palmitoylation in these neurons that has yet to be explored.  
450 Accordingly, many of the key proteins involved in cholinergic synaptic transmission are S-palmitoylation  
451 substrates including muscarinic acetylcholine receptor M2 (CHRM2), acetylcholinesterase (ACHE) and  
452 ATP-citrate synthase (ACLY; Blanc et al., 2015, 2019). Our observations of co-enrichment of certain  
453 palmitoylating and de-palmitoylating enzymes are also of interest, such as *Abhd17b* and *Zdhhc9* in  
454 oligodendrocytes. It is possible that these enzymes share substrates to mediate dynamic palmitoylation,  
455 or have separate substrates in order to maintain stable S-palmitoylation states of certain oligodendrocyte  
456 expressed proteins. Importantly, the data accessibility in BrainPalmSeq will enable researchers to develop  
457 hypotheses regarding their cell type, brain region or protein of interest.

458 The palmitoylome of each cell type in the nervous system is likely to be highly heterogeneous and  
459 will be determined by the expression of both the S-palmitoylation substrates and the palmitoylating and  
460 de-palmitoylating enzymes in a given cell type. Furthermore, accumulating evidence has revealed that  
461 this palmitoylome can be altered by extrinsic factors such as chronic stress and neuronal activity (Kang et  
462 al., 2008; Zareba-Kozioł et al., 2019). While we have provided predicted palmitoylomes composed of

463 several highly expressed or enriched S-palmitoylation substrates in select brain regions and cell types,  
464 experimental validation to reveal the relative palmitoylation of substrates under various conditions is  
465 needed to fully understand these cellular differences. Nevertheless, we were able utilize our predicted  
466 palmitoylomes to validate substrates for ZDHHC9, giving insight into the potential role of this enzyme in  
467 myelin regulation in the brain.

468 Neurological disorders that arise from LOF gene mutations might be predicted to lead to  
469 pathological changes that are more severe in the brain regions in which these genes are most highly  
470 expressed. We observed this type of regional overlay for the expression patterns of *Zdhhc8*, *Zdhhc9* and  
471 *Ppt1*. Numerous other brain disorders are thought to be exacerbated by an imbalance in S-palmitoylation,  
472 such as decreased S-palmitoylation of HTT in huntington's disease (Virlogeux et al., 2021; Yanai et al.,  
473 2006), increased S-palmitoylation of APP and TAU in Alzheimer's disease (Cho and Park, 2016), and  
474 decreased S-palmitoylation of 5-HTA receptor in major depressive disorder (Gorinski et al., 2019). Efforts  
475 are already underway to normalize aberrant palmitoylation in neurological diseases in order to improve  
476 clinical outcomes (Roberts et al., 2012; Virlogeux et al., 2021). Understanding the brain expression  
477 patterns of the enzymes that mediate palmitoylation in these diseases will be key to developing and  
478 targeting such therapeutics.

#### 479 **Differential gene expression as a means to control S-palmitoylation in the brain**

480 The mechanisms that govern ZDHHC enzyme-substrate interactions are complex and still not fully  
481 understood. While the majority of post-translational modifications including phosphorylation and N-  
482 glycosylation are highly sequence specific (Schwarz and Aebi, 2011; Ubersax and Ferrell, 2007), several  
483 studies have revealed that S-palmitoylation by ZDHHCs can be stochastic, proximity based and lacking in  
484 stereo-selectivity (Rocks et al., 2010; Rodenburg et al., 2017). Contrasting studies have shown that  
485 numerous ZDHHCs have specific protein interacting domains including ankyrin repeat (AR), PDZ and SH3  
486 domains that facilitate substrate interactions, providing support for a model in which more specific  
487 enzyme-substrate interactions can govern S-palmitoylation (Abrami et al., 2017; Lemonidis et al., 2015;  
488 Plain et al., 2020; Rana et al., 2018; Thomas et al., 2012; Verardi et al., 2017). Furthermore, a recent study  
489 found striking substrate specificity for several ZDHHCs with the G-protein subunit G $\alpha$ , and revealed  
490 intriguing observations that the subcellular localization of a number of S-palmitoylation substrates could  
491 be controlled by changing the localization, and importantly, the expression of certain ZDHHC enzymes. In  
492 this study, S-palmitoylated substrates accumulated in the subcellular compartment in which their partner  
493 ZDHHCs were targeted (Solis et al., 2020). This is particularly relevant as the ZDHHCs are known to have



494 diverse subcellular localizations including the golgi, ER, endosomes and plasma membrane (Globa and  
495 Bamji, 2017). Transcriptional control of differentially compartmentalized palmitoylating and de-  
496 palmitoylating enzymes could therefore be an essential mechanism for regulating the subcellular  
497 localization, and function, of *S*-palmitoylated protein substrates. Accordingly, LOF mutations in certain  
498 ZDHHC enzymes leads to cell type-specific disruption in *S*-palmitoylation that is not compensated by other  
499 members of the large ZDHHC family. We provide a means to investigate the expression of the proteins  
500 that mediate *S*-palmitoylation, making BrainPalmSeq an invaluable resource to both researchers and  
501 clinicians that are working to better understand the role of *S*-palmitoylation in the brain.

502

503 **Supplementary Tables**

504 [https://docs.google.com/spreadsheets/d/1egtQL5tY5WolePrv2757Mxwrkcm1hc5gQycOvmsvKdk/edit?u](https://docs.google.com/spreadsheets/d/1egtQL5tY5WolePrv2757Mxwrkcm1hc5gQycOvmsvKdk/edit?usp=sharing)  
505 [sp=sharing](https://docs.google.com/spreadsheets/d/1egtQL5tY5WolePrv2757Mxwrkcm1hc5gQycOvmsvKdk/edit?usp=sharing)

506

507 **Figure Legends**

508 **Figure 1. Heterogeneous ZDHHC expression in the mouse nervous system**

509 (A) Heatmap showing expression for the 24 ZDHHC genes, extracted from scRNAseq study of mouse CNS  
510 and PNS (Zeisel et al., 2018). Each column represents one of the 265 metacells classified in the study.  
511 Metacells are organized along x-axis according to hierarchical clustering designations generated by Zeisel  
512 et al. Full metadata for this study available on BrainPalmSeq.

513 (B) Heatmap showing mean ZDHHC expression per hierarchical cluster, with columns and rows sorted by  
514 descending mean ZDHHC expression per row/column.

515 (C) Heatmap showing mean ZDHHC expression per neurotransmitter cluster for all PNS and CNS neurons.  
516 Columns and rows are sorted as in B.

517 (D) Correlation network showing ZDHHC co-expression across all metacells in 'MouseBrain' (Spearman R  
518 > 0.5). Numbers in nodes correspond to ZDHHC number. Node color represents mean expression across  
519 all metacells. Edge thickness represents strength of correlation.

520 (E) Graph showing proportion of genes from 'MouseBrain' dataset that are co-expressed with one or more  
521 ZDHHC and also substrates for S-palmitoylation (SwissPalm annotated). 'Brain expressed' = 15,389 protein  
522 coding genes expressed in the postnatal mouse brain, curated from the MGI RNAseq studies database. 'R  
523 > 0.7 ZDHHC co-expressed' = 914 genes co-expressed with one or more ZDHHC (Spearman R > 0.7). 'R >  
524 0.8 ZDHHC co-expressed' = list of 167 genes co-expressed with one or more ZDHHC (Spearman R > 0.8).  
525 Brain expressed vs. R > 0.7: p < 0.001; R > 0.7 vs R > 0.8: p < 0.01; Fisher's exact test.

526 (F) Graph of GO biological process analysis. Gene IDs from the 'MouseBrain' dataset (Zeisel et al., 2018)  
527 that showed correlated expression with one or more ZDHHC (R > 0.7) and were also Uniprot reviewed and  
528 SwissPalm annotated were used as input.

529 Units for all heatmaps in figure: mean log<sub>2</sub>(counts per 10,000 + 1).

530 **Figure 2. Diversity in ZDHHC expression and S-palmitoylation substrate expression in the hippocampus**

531 (A) Heatmap of excitatory neuron ZDHHC expression from dorsal hippocampus (original pooled cell  
532 RNAseq data from Cembrowski et al., 2016) projected onto diagrams of dorsal hippocampus.

533 (B) Hierarchical clustering of ZDHHC expression data in A.

534 (C) Heatmap showing top 6 ranked expressing ZDHHCs in dorsal CA1 in descending order.

535 (D) Pie chart showing proportion genes with enriched expression in dorsal CA1 (dCA1) that are also  
536 substrates for palmitoylation (SwissPalm annotated).

537 (E) KEGG analysis of the dCA1 enriched/SwissPalm annotated genes.

538 (F) SynGO analysis of the dCA1 enriched/SwissPalm annotated genes.

539 (G-J) As in (C)-(F) but for the dorsal dentate gyrus (dDG).

540 Heatmap legend in (A) applies to all heatmaps (logFKPM).

541 **Figure 3. Pyramidal neuron layer specific ZDHHC expression**

542 (A) Heatmap of excitatory neuron ZDHHC expression from somatosensory cortex (original data scRNAseq  
543 data from Zeisel et al., 2015) projected onto diagrams of cortical layers.

544 (B) Hierarchical clustering of ZDHHC expression data in A. Heatmap units in (A, B): mean log<sub>2</sub>(counts per  
545 10,000 + 1)

546 (C) Heatmap of scRNAseq data from Allen Brain 10X genomics (Yao et al., 2021). Data are represented as  
547 mean ZDHHC expression per excitatory neuron subtype, with columns and rows sorted by descending  
548 mean ZDHHC expression per row/column.

549 (D) As in (C) but for inhibitory neuron subtypes. Heatmap units for (C, D):

550 **Figure 4. Heterogeneous de-palmitoylating enzyme and ZDHHC accessory protein expression in the**  
551 **mouse nervous system**

552 (A) Heatmap showing expression of de-palmitoylating enzymes (top) and ZDHHC accessory subunits  
553 (bottom), extracted from scRNAseq study of mouse CNS and PNS (Zeisel et al., 2018). Each column  
554 represents one of the 265 metacells classified in the study. Metacells are organized according to  
555 hierarchical clustering designations generated by Zeisel et al.

556 (B) Heatmap showing mean de-palmitoylating enzyme expression per hierarchical cluster, with columns  
557 and rows sorted by descending mean ZDHHC expression per row/column.

558 (C) As B but for ZDHHC accessory proteins.

559 (D) Correlation network showing ZDHHC co-expression with de-palmitoylating enzymes and accessory  
560 proteins across all metacells in 'MouseBrain' (Spearman R > 0.4). Node color represents mean expression  
561 across all metacells. Edge thickness represents strength of correlation.

562 **Figure 5. Disease associated palmitoylating enzyme regional and cell-type expression overlays with**  
563 **brain pathology in associated LOF disorders**

564 (A) Heatmap showing ranked *Zdhhc8* expressing neuronal and glial cell types in descending order. Original  
565 data from scRNAseq neonatal mouse brain study; Rosenberg et al., 2018. Cell types were averaged as  
566 described in Table SY. Heatmap units: log<sub>2</sub>(TPM+1).

567 (B) As in A but original data from scRNAseq adolescent mouse brain study Zeisel et al (2018). Heatmap  
568 units: mean log<sub>2</sub>(counts per 10,000 + 1).

569 (C) Heatmap of *Zdhhc8* expression from whole brain regional bulk RNAseq data (original data from  
570 'Protein Atlas'; Sjöstedt et al., 2020) projected onto anatomical map of mouse brain. Heatmap units:  
571 FKPM.

572 (D-F) As in (A)-(C) but for *Zdhhc9*.

573 (G-I) As in (A)-(C) but for *Ppt1*.

574 **Figure 6. Validation of predicted S-palmitoylation substrates of *Zdhhc9* derived from cell-type**  
575 **enriched expression**

576 (A) Graph of expression data for *Zdhhc9* extracted from BrainPalmSeq. Original data from oligodendrocyte  
577 scRNAseq study by Marques et al. Expression units: mean  $\log_2(\text{counts per } 10,000 + 1)$ .

578 (B) Diagram illustrating workflow to generate a list of oligodendrocyte enriched palmitoylation  
579 substrates, GO annotated for myelin sheath for experimental validation.

580 (C) STRING diagram of myelin sheath annotated palmitoylation substrates.

581 (D) Western blot following Acyl-RAC palmitoylation assay in HEK293 cells to identify palmitoylated and  
582 unpalmitoylated fractions of FLAG-MOBP either without or with co-transfection of FLAG-GOLGA7 and  
583 HA-ZDHHC9. Input = unprocessed protein lysate. NSB control = non-specific binding of unpalmitoylated  
584 protein to sepharose resin in control pipeline. Palm fraction = palmitoylated protein (bound to  
585 sepharose resin). Unpalm fraction = unpalmitoylated protein (did not bind to sepharose resin).

586 (E-F) As in (D) but for FLAG-PLP1 or FLAG-CNP.

587 (G) Graphs quantifying the ratio of palmitoylated to unpalmitoylated protein either with or without co-  
588 transfusions with FLAG-GOLGA7 and HA-ZDHHC9. n = 4-6 cultures per condition. \*\* p < 0.01, \*\*\* p <  
589 0.001; two-way ANOVA; Šídák's post hoc; mean  $\pm$  SEM.

590

## 591 **Materials and Methods**

### 592 **Data processing for BrainPalmSeq**

593 For Zeisel et al., 2018 ('MouseBrain'), single-cell counts (UMI from 3' end counting) were downloaded  
594 from MouseBrain.org (loom file named I5\_all.loom), and log normalized by first scaling the expression  
595 values provided to a sum of 10,000 per cell before calculating  $\log_2(\text{scaled\_counts}+1)$ . Averages were then  
596 performed by brain region, neurotransmitter and taxonomy for each gene.

597 For DropViz Metacell counts were downloaded from DropViz.org (count file  
598 metacells.BrainCellAtlas\_Saunders\_version\_2018.04.01.RDS and annotation file  
599 annotation.BrainCellAtlas\_Saunders\_version\_2018.04.01.RDS) and log normalized by first scaling the  
600 expression values provided to a sum of 10,000 per metacell before calculating  $\log_2(\text{scaled\_counts}+1)$ .  
601 Averages were then performed by cell type, tissue and class for each gene. Genes associated with  
602 palmitoylation were selected in order to create the heatmaps.

603 For Zeisel, Single-cell counts (UMI from 3' end counting) were downloaded from  
604 [https://storage.googleapis.com/linnarsson-lab-www-blobs/blobs/cortex/expression\\_mRNA\\_17-Aug-](https://storage.googleapis.com/linnarsson-lab-www-blobs/blobs/cortex/expression_mRNA_17-Aug-2014.txt)  
605 [2014.txt](https://storage.googleapis.com/linnarsson-lab-www-blobs/blobs/cortex/expression_mRNA_17-Aug-2014.txt), and log normalized by first scaling the expression values provided to a sum of 10,000 per cell  
606 before calculating  $\log_2(\text{scaled\_counts}+1)$ . Averages were then performed by cluster, tissue and class for  
607 each gene. Genes associated with palmitoylation were selected in order to create the heatmaps,  
608 categories comprising fewer than 5 single cells are not displayed.

609 Marques, Single-cell counts (UMI from 3' end counting) were downloaded from GEO with accession ID  
610 GSE75330 (file GSE75330\_Marques\_et\_al\_mol\_counts2.tab) and log normalized by first scaling the  
611 expression values provided to a sum of 10,000 per cell before calculating  $\log_2(\text{scaled\_counts}+1)$ . Averages  
612 were then performed by cluster and region for each gene. Genes associated with palmitoylation were  
613 selected in order to create the heatmaps, categories comprising fewer than 5 single cells are not displayed.

614 For Rosenberg single-cell counts (UMI from 3' end counting) were downloaded from GSE110823, and log  
615 normalized by first scaling the expression values provided to a sum of 10,000 per cell before calculating  
616  $\log_2(\text{scaled\_counts}+1)$ . Averages were then performed by brain region, neurotransmitter and taxonomy  
617 for each gene. Genes associated with palmitoylation were selected in order to create the heatmaps.

618 Data from Sjöstedt et al. were downloaded as Protein-coding transcripts per million (pTPM) from  
619 [proteinatlas.org](https://proteinatlas.org/) ("RNA mouse brain region gene data") and not further processed.

620 For Hipposeq, expression data were downloaded as FKPM directly from [hipposeq.janelia.org](https://hipposeq.janelia.org/) and were  
621 not further processed.

622 For Allen Brain 10X data, expression data were downloaded as trimmed means (25%-75%)  $\log_2(\text{CPM}+1)$   
623 from [portal.brain-map.org/](https://portal.brain-map.org/) and were not further processed.

### 624 **Correlation analysis**

625 Spearman correlation values between genes and their significances were calculated in R using the  
626 expression results obtained for each cell type as described above.

## 627 **Identification of S-palmitoylation substrates with SwissPalm**

628 Gene lists were inputted into SwissPalm (<https://swisspalm.org/proteins>) input file function and cross-  
629 referenced with 'Dataset 3: Palmitoylation validated or found in at least one palmitoyl-proteome  
630 (SwissPalm annotated)' for Mus Musculus, with an additional filter for UniProt 'Reviewed' proteins.

## 631 **Generating a predicted palmitoylome for dorsal hippocampus**

632 To curate the regionally enriched predicted-palmitoylome, the enrichment analysis tools in hipposeq  
633 (<https://hipposeq.janelia.org/>) were used to compare each of the selected Cell Lines vs the other Cell Lines  
634 in the analysis (Selected Cell Lines = dorsal DG, CA3, CA2 and CA1), with the following parameters: 'Fold  
635 threshold' = 1.5; 'FKPMmin threshold' = 5, 'FDR' = 0.05. The resulting lists of regionally enriched transcripts  
636 were cross referenced with SwissPalm as described above to identify regionally enriched S-palmitoylation  
637 substrates.

## 638 **Bioinformatic analysis**

639 Gene Ontology (GO) analysis was performed using statistical overrepresentation tests in PANTHER16.0  
640 (Mi et al., 2009) with default settings and mus musculus as the reference species. Biological process GO  
641 terms were extracted and ranked according to false discovery rate (FDR). Kyoto Encyclopedia of Genes  
642 and Genomes (KEGG) analysis was performed using the web-based program Enrichr (Chen et al., 2013;  
643 Kuleshov et al., 2016) and ranked according to -log Adjusted P-value. Synaptic Gene Ontologies (SynGO;  
644 version 1.1) analysis was performed using default settings with brain expressed genes as a background  
645 and and terms for 'biological process' were ranked according to -log Adjusted P-value. Functional protein  
646 interaction networks were identified using the Search Tool for the Retrieval of Interacting Genes (STRING)  
647 11.0 (Szklarczyk et al., 2019) with mus musculus as the reference species. Seven types of protein  
648 interactions were used for network generation, including text mining, neighborhood, co-occurrence, co-  
649 expression, gene fusion, experiments and databases.

## 650 **Data presentation**

651 Heatmaps were plotted and hierarchical clustering performed in Displayr (<https://www.displayr.com>)  
652 using the 'Dendrogram' function. Cytoscape (Version 3.8.0) was used to draw correlation networks.

## 653 **Heatmap creation for BrainPalmSeq**

654 All plots for the BrainPalmSeq database were generated using curated RNA sequencing datasets. Python  
655 3 and Javascript scripts were used with the plotting library Bokeh to generate the interactive heatmaps to  
656 display and compare these datasets on the BrainPalmSeq website (Bokeh Development Team, 2018).

## 657 **Cell culture**

658 HEK293T cells were thawed and aliquoted into a 10cm dish with 10mL prewarmed (37°C) DMEM  
659 (GIBCO, Thermo Fisher Scientific, Waltham, MA) supplemented with 10% fetal bovine serum (FBS)  
660 (GIBCO, Thermo Fisher Scientific, Waltham, MA) and 1% Pen/Strep(P/S) (GIBCO, Thermo Fisher  
661 Scientific, Waltham, MA). HEK293T cells were then placed in a 37°C incubator with 5% CO<sub>2</sub> and  
662 passaged approximately every 5 days, or once confluency was achieved.

## 663 **Transfection**

664 70%-80% confluent HEK293T cells were transfected using Lipofectamine 2000 (Invitrogen/Life  
665 Technologies, Carlsbad, CA) according to the manufacturer's recommendations. Each well of a 6-well  
666 plate was transfected with a total of 3ug DNA, 150uL of Opti-Mem (GIBCO, Thermo Fisher Scientific,  
667 Waltham, MA) was used with 6uL of Lipofectamine 2000 (Invitrogen/Life Technologies, Carlsbad, CA).  
668 Experimental condition wells were transfected with 1ug of the indicated construct of interest, 1ug of  
669 HA-DHHC9 (mouse; Shimell et al., 2019), and 1ug of FLAG-GOLGA7 (Maurine Linder, Washington  
670 University School of Medicine). Human FLAG-MOBP (CAT#: RC223946), FLAG-PLP1 (CAT#: RC218616)  
671 and FLAG-CNP (CAT#: RC207038) were acquired from Origene, Maryland, USA. Control condition wells  
672 were transfected with 1ug of the indicated construct of interest, and 2ug of a scrambled control  
673 plasmid. Cells were lysed using the acyl-RAC assay lysis buffer 48hours after transfection.

## 674 **Palmitoylation Assay (acyl-RAC)**

675 The commercially available CAPTUREome S-palmitoylated protein kit (Badrilla, Leeds, UK) was used in  
676 accordance with the manufacturer's guidelines with three optimizations: (1) prior to the cell lysis step,  
677 wells were washed with 1mL of 1X PBS to eliminate any dead cells or residual media; (2) during the cell  
678 lysis step, DNase (Sigma-Aldrich, St. Louis, MO), was added to the solution (5uL per 500uL of lysis  
679 buffer); and (2) protein concentration was measured prior to the separation of experimental sample and  
680 negative control sample using the BCA Assay (Pierce, Thermo Fisher Scientific, Waltham, MA).

## 681 **Western Blot Analysis**

682 Western blotting was performed using 4% stacking and 12% resolving SDS-PAGE gels. PVDF membranes  
683 were then blocked for 1hour at room temperature with 5% BSA in 0.05% TBS-T. PVDF membranes were  
684 incubated with the indicated primary antibodies (anti-HA: Cell Signaling Technology, C29F4, Rabbit mAb  
685 CAT#: 3724, 1:1000; anti-FLAG: Origene, mouse monoclonal antibody, CAT#: TA50011-100, 1:1000)  
686 overnight at 4°C. Proteins were then visualized using enhanced chemiluminescence (Immubilon Western  
687 Chemiluminescent HRP Substrate) on a BioRad ChemiDoc XRS+ scanner. Blots were then quantified  
688 using Fiji1 software. The palmitoylated and unpalmitoylated fractions were calculated using the  
689 following equations respectively: (Palm Fraction / (Palm Fraction + Unpalm Fraction)) and (Unpalm  
690 Fraction / (Palm Fraction + Unpalm Fraction)). Statistical analyses were performed in GraphPad Prism  
691 9.2.0.

## 692 **Acknowledgements**

693 The authors would like to thank Drs. A Ciernia, M Cembrowski, T Murphy and J LeDue for helpful  
694 discussion.

695 **References**

- 696 Abrami L, Dallavilla T, Sandoz PA, Demir M, Kunz B, Savoglidis G, Hatzimanikatis V, van Der Goot FG.  
697 2017. Identification and dynamics of the human ZDHC16-ZDHC6 palmitoylation cascade. *eLife* **6**.  
698 doi:10.7554/eLife.27826
- 699 Baker K, Astle DE, Scerif G, Barnes J, Smith J, Moffat G, Gillard J, Baldeweg T, Raymond FL. 2015.  
700 Epilepsy, cognitive deficits and neuroanatomy in males with ZDHC9 mutations. *Annals of Clinical*  
701 *and Translational Neurology* **2**:559–569. doi:10.1002/acn3.196
- 702 Bathelt J, Astle D, Barnes J, Raymond FL, Baker K. 2016. Structural brain abnormalities in a single gene  
703 disorder associated with epilepsy, language impairment and intellectual disability. *NeuroImage:*  
704 *Clinical* **12**:655–665. doi:10.1016/j.nicl.2016.07.016
- 705 Bathelt J, Barnes J, Raymond FL, Baker K, Astle D. 2017. Global and Local Connectivity Differences  
706 Converge With Gene Expression in a Neurodevelopmental Disorder of Known Genetic Origin.  
707 *Cerebral Cortex* **27**:3806–3817. doi:10.1093/cercor/bhx027
- 708 Bird CM, Burgess N. 2008. The hippocampus and memory: Insights from spatial processing. *Nature*  
709 *Reviews Neuroscience* **9**:182–194. doi:10.1038/nrn2335
- 710 Blanc M, David F, Abrami L, Migliozi D, Armand F, Bürgi J, van der Goot FG. 2015. SwissPalm: Protein  
711 Palmitoylation database. *F1000Research* **4**. doi:10.12688/f1000research.6464.1
- 712 Blanc M, David FPA, van der Goot FG. 2019. SwissPalm 2: Protein S-palmitoylation database Methods in  
713 Molecular Biology. Humana Press Inc. pp. 203–214. doi:10.1007/978-1-4939-9532-5\_16
- 714 Chen EY, Tan CM, Kou Y, Duan Q, Wang Z, Meirelles G V., Clark NR, Ma’ayan A. 2013. Enrichr: Interactive  
715 and collaborative HTML5 gene list enrichment analysis tool. *BMC Bioinformatics* **14**.  
716 doi:10.1186/1471-2105-14-128
- 717 Chen WY, Shi YY, Zheng YL, Zhao XZ, Zhang GJ, Chen SQ, Yang P Di, He L. 2004. Case-control study and  
718 transmission disequilibrium test provide consistent evidence for association between  
719 schizophrenia and genetic variation in the 22q11 gene ZDHC8. *Human Molecular Genetics*  
720 **13**:2991–2995. doi:10.1093/hmg/ddh322
- 721 Cho E, Park M. 2016. Palmitoylation in Alzheimer’s disease and other neurodegenerative diseases.  
722 *Pharmacological Research* **111**:133–151. doi:10.1016/j.phrs.2016.06.008



- 723 Forrester MT, Hess DT, Thompson JW, Hultman R, Moseley MA, Stamler JS, Casey PJ. 2011. Site-specific  
724 analysis of protein S-acylation by resin-assisted capture. *Journal of Lipid Research* **52**:393–398.  
725 doi:10.1194/JLR.D011106/ATTACHMENT/AA2B322B-A63D-41C0-A864-92DAC7C09076/MMC1.PDF
- 726 Fredericks G, Hoffmann F, Hondal R, Rozovsky S, Urschitz J, Hoffmann P. 2017. Selenoprotein K Increases  
727 Efficiency of DHH6 Catalyzed Protein Palmitoylation by Stabilizing the Acyl-DHH6 Intermediate.  
728 *Antioxidants* **7**:4. doi:10.3390/antiox7010004
- 729 Fredericks GJ, Hoffmann FKW, Rose AH, Osterheld HJ, Hess FM, Mercier F, Hoffmann PR. 2014. Stable  
730 expression and function of the inositol 1,4,5-triphosphate receptor requires palmitoylation by a  
731 DHH6/selenoprotein K complex. *Proceedings of the National Academy of Sciences of the United*  
732 *States of America* **111**:16478–16483. doi:10.1073/pnas.1417176111
- 733 Fukata Y, Dimitrov A, Boncompain G, Vielemeyer O, Perez F, Fukata M. 2013. Local palmitoylation cycles  
734 define activity-regulated postsynaptic subdomains. *Journal of Cell Biology* **202**:145–161.  
735 doi:10.1083/jcb.201302071
- 736 Fukata Y, Fukata M. 2010. Protein palmitoylation in neuronal development and synaptic plasticity.  
737 *Nature Reviews Neuroscience* **11**:161–175. doi:10.1038/nrn2788
- 738 Glantz LA, Lewis DA. 2000. Decreased dendritic spine density on prefrontal cortical pyramidal neurons in  
739 schizophrenia. *Archives of General Psychiatry* **57**:65–73. doi:10.1001/archpsyc.57.1.65
- 740 Globa AK, Bamji SX. 2017. Protein palmitoylation in the development and plasticity of neuronal  
741 connections. *Current Opinion in Neurobiology* **45**:210–220. doi:10.1016/j.conb.2017.02.016
- 742 Gorinski N, Bijata M, Prasad S, Wirth A, Abdel Galil D, Zeug A, Bazovkina D, Kondaurova E, Kulikova E,  
743 Ilchibaeva T, Zareba-Kozioł M, Papaleo F, Scheggia D, Kochlamazashvili G, Dityatev A, Smyth I,  
744 Krzystyniak A, Włodarczyk J, Richter DW, Strekalova T, Sigrist S, Bang C, Hobuß L, Fiedler J, Thum T,  
745 Naumenko VS, Pandey G, Ponimaskin E. 2019. Attenuated palmitoylation of serotonin receptor 5-  
746 HT1A affects receptor function and contributes to depression-like behaviors. *Nature*  
747 *Communications* **10**:1–14. doi:10.1038/s41467-019-11876-5
- 748 Haque A, Engel J, Teichmann SA, Lönnberg T. 2017. A practical guide to single-cell RNA-sequencing for  
749 biomedical research and clinical applications. *Genome Medicine* **9**:1–12. doi:10.1186/s13073-017-  
750 0467-4

- 751 Harris KD, Shepherd GMG. 2015. The neocortical circuit: Themes and variations. *Nature Neuroscience*  
752 **18**:170–181. doi:10.1038/nn.3917
- 753 Ji B, Skup M. 2021. Roles of palmitoylation in structural long-term synaptic plasticity. *Molecular Brain*  
754 **14**:1–27. doi:10.1186/s13041-020-00717-y
- 755 Kang R, Wan J, Arstikaitis P, Takahashi H, Huang K, Bailey AO, Thompson JX, Roth AF, Drisdell RC, Mastro  
756 R, Green WN, Yates JR, Davis NG, El-Husseini A. 2008. Neural palmitoyl-proteomics reveals dynamic  
757 synaptic palmitoylation. *Nature* **456**:904–909. doi:10.1038/nature07605
- 758 Karayiorgou M, Simon TJ, Gogos JA. 2010. 22q11.2 microdeletions: Linking DNA structural variation to  
759 brain dysfunction and schizophrenia. *Nature Reviews Neuroscience* **11**:402–416.  
760 doi:10.1038/nrn2841
- 761 Kolluri N, Sun Z, Sampson AR, Lewis DA. 2005. Lamina-specific reductions in dendritic spine density in  
762 the prefrontal cortex of subjects with schizophrenia. *American Journal of Psychiatry* **162**:1200–  
763 1202. doi:10.1176/appi.ajp.162.6.1200
- 764 Koopmans F, van Nierop P, Andres-Alonso M, Byrnes A, Cijssouw T, Coba MP, Cornelisse LN, Farrell RJ,  
765 Goldschmidt HL, Howrigan DP, Hussain NK, Imig C, de Jong APH, Jung H, Kohansalnodehi M,  
766 Kramarz B, Lipstein N, Lovering RC, MacGillavry H, Mariano V, Mi H, Ninov M, Osumi-Sutherland D,  
767 Pielot R, Smalla KH, Tang H, Tashman K, Toonen RFG, Verpelli C, Reig-Viader R, Watanabe K, van  
768 Weering J, Achsel T, Ashrafi G, Asi N, Brown TC, De Camilli P, Feuermann M, Foulger RE, Gaudet P,  
769 Joglekar A, Kanellopoulos A, Malenka R, Nicoll RA, Pulido C, de Juan-Sanz J, Sheng M, Südhof TC,  
770 Tilgner HU, Bagni C, Bayés À, Biederer T, Brose N, Chua JJE, Dieterich DC, Gundelfinger ED,  
771 Hoogenraad C, Hugarir RL, Jahn R, Kaeser PS, Kim E, Kreutz MR, McPherson PS, Neale BM,  
772 O'Connor V, Posthuma D, Ryan TA, Sala C, Feng G, Hyman SE, Thomas PD, Smit AB, Verhage M.  
773 2019. SynGO: An Evidence-Based, Expert-Curated Knowledge Base for the Synapse. *Neuron*  
774 **103**:217-234.e4. doi:10.1016/j.neuron.2019.05.002
- 775 Koster KP, Yoshii A. 2019. Depalmitoylation by palmitoyl-protein thioesterase 1 in neuronal health and  
776 degeneration. *Frontiers in Synaptic Neuroscience* **11**:25. doi:10.3389/fnsyn.2019.00025
- 777 Kouskou M, Thomson DM, Brett RR, Wheeler L, Tate RJ, Pratt JA, Chamberlain LH. 2018. Disruption of  
778 the *Zdhhc9* intellectual disability gene leads to behavioural abnormalities in a mouse model.  
779 *Experimental Neurology* **308**:35–46. doi:10.1016/J.EXPNEUROL.2018.06.014

- 780 Kuleshov M V., Jones MR, Rouillard AD, Fernandez NF, Duan Q, Wang Z, Koplev S, Jenkins SL, Jagodnik  
781 KM, Lachmann A, McDermott MG, Monteiro CD, Gundersen GW, Ma'ayan A. 2016. Enrichr: a  
782 comprehensive gene set enrichment analysis web server 2016 update. *Nucleic acids research*  
783 **44**:W90–W97. doi:10.1093/nar/gkw377
- 784 Lemonidis K, Sanchez-Perez MC, Chamberlain LH. 2015. Identification of a novel sequence motif  
785 recognized by the ankyrin repeat domain of zDHHC17/13 S-acyltransferases. *Journal of Biological*  
786 *Chemistry* **290**:21939–21950. doi:10.1074/jbc.M115.657668
- 787 Lin DTS, Conibear E. 2015. ABHD17 proteins are novel protein depalmitoylases that regulate N-Ras  
788 palmitate turnover and subcellular localization. *eLife* **4**. doi:10.7554/eLife.11306
- 789 Lu JY, Verkruyse LA, Hofmann SL. 1996. Lipid thioesters derived from acylated proteins accumulate in  
790 infantile neuronal ceroid lipofuscinosis: Correction of the defect in lymphoblasts by recombinant  
791 palmitoyl-protein thioesterase. *Proceedings of the National Academy of Sciences of the United*  
792 *States of America* **93**:10046–10050. doi:10.1073/pnas.93.19.10046
- 793 Ma Y, Liu H, Ou Z, Qi C, Xing R, Wang S, Han Y, Zhao T-J, Chen Y. 2021. DHHC5 facilitates oligodendrocyte  
794 development by palmitoylating and activating STAT3. *Glia*. doi:10.1002/glia.24113
- 795 Malgapo MIP, Linder ME. 2021. Substrate recruitment by zDHHC protein acyltransferases. *Open Biology*  
796 **11**:rsob.210026. doi:10.1098/rsob.210026
- 797 Marques S, Zeisel A, Codeluppi S, Van Bruggen D, Falcão AM, Xiao L, Li H, Häring M, Hochgerner H,  
798 Romanov RA, Gyllborg D, Muñoz-Manchado AB, La Manno G, Lönnerberg P, Floriddia EM, Rezayee  
799 F, Ernfors P, Arenas E, Hjerling-Leffler J, Harkany T, Richardson WD, Linnarsson S, Castelo-Branco G.  
800 2016. Oligodendrocyte heterogeneity in the mouse juvenile and adult central nervous system.  
801 *Science* **352**:1326–1329. doi:10.1126/science.aaf6463
- 802 Matt L, Kim K, Chowdhury D, Hell JW. 2019. Role of palmitoylation of postsynaptic proteins in promoting  
803 synaptic plasticity. *Frontiers in Molecular Neuroscience*. doi:10.3389/fnmol.2019.00008
- 804 Mi H, Dong Q, Muruganujan A, Gaudet P, Lewis S, Thomas PD. 2009. PANTHER version 7: Improved  
805 phylogenetic trees, orthologs and collaboration with the Gene Ontology Consortium. *Nucleic Acids*  
806 *Research* **38**. doi:10.1093/nar/gkp1019
- 807 Mitchell DA, Hamel LD, Reddy KD, Farh L, Rettew LM, Sanchez PR, Deschenes RJ. 2014. Mutations in the

- 808 X-linked intellectual disability gene, zDHHC9, alter autopalmitoylation activity by distinct  
809 mechanisms. *Journal of Biological Chemistry* **289**:18582–18592. doi:10.1074/jbc.M114.567420
- 810 Mukai J, Liu H, Burt RA, Swor DE, Lai WS, Karayiorgou M, Gogos JA. 2004. Evidence that the gene  
811 encoding ZDHHC8 contributes to the risk of schizophrenia. *Nature Genetics* **36**:725–731.  
812 doi:10.1038/ng1375
- 813 Nita DA, Mole SE, Minassian BA. 2016. Neuronal ceroid lipofuscinoses. *Epileptic Disorders* **18**:S73–S88.  
814 doi:10.1684/epd.2016.0844
- 815 Pitts MW, Hoffmann PR. 2018. Endoplasmic reticulum-resident selenoproteins as regulators of calcium  
816 signaling and homeostasis. *Cell Calcium* **70**:76–86. doi:10.1016/j.ceca.2017.05.001
- 817 Plain F, Howie J, Kennedy J, Brown E, Shattock MJ, Fraser NJ, Fuller W. 2020. Control of protein  
818 palmitoylation by regulating substrate recruitment to a zDHHC-protein acyltransferase.  
819 *Communications Biology* **3**:1–10. doi:10.1038/s42003-020-01145-3
- 820 Rana MS, Lee CJ, Banerjee A. 2018. The molecular mechanism of DHHC protein acyltransferases.  
821 *Biochemical Society Transactions* **47**:157–167. doi:10.1042/BST20180429
- 822 Raymond FL, Tarpey PS, Edkins S, Tofts C, O’Meara S, Teague J, Butler A, Stevens C, Barthorpe S, Buck G,  
823 Cole J, Dicks E, Gray K, Halliday K, Hills K, Hinton J, Jones D, Menzies A, Perry J, Raine K, Shepherd R,  
824 Small A, Varian J, Widaa S, Mallya U, Moon J, Luo Y, Shaw M, Boyle J, Kerr B, Turner G, Quarrell O,  
825 Cole T, Easton DF, Wooster R, Bobrow M, Schwartz CE, Gecz J, Stratton MR, Futreal PA. 2007.  
826 Mutations in ZDHHC9, Which Encodes a Palmitoyltransferase of NRAS and HRAS, Cause X-Linked  
827 Mental Retardation Associated with a Marfanoid Habitus. *The American Journal of Human Genetics*  
828 **80**:982–987. doi:10.1086/513609
- 829 Roberts MS, Macauley SL, Wong AM, Yilmaz D, Hohm S, Cooper JD, Sands MS. 2012. Combination small  
830 molecule PPT1 mimetic and CNS-directed gene therapy as a treatment for infantile neuronal ceroid  
831 lipofuscinosis. *Journal of Inherited Metabolic Disease* **35**:847–857. doi:10.1007/s10545-011-9446-x
- 832 Rocks O, Gerauer M, Vartak N, Koch S, Huang ZP, Pechlivanis M, Kuhlmann J, Brunsveld L, Chandra A,  
833 Ellinger B, Waldmann H, Bastiaens PIH. 2010. The palmitoylation machinery is a spatially organizing  
834 system for peripheral membrane proteins. *Cell* **141**:458–471. doi:10.1016/j.cell.2010.04.007
- 835 Rodenburg RNP, Snijder J, Van De Waterbeemd M, Schouten A, Granneman J, Heck AJR, Gros P. 2017.

- 836 Stochastic palmitoylation of accessible cysteines in membrane proteins revealed by native mass  
837 spectrometry. *Nature Communications* **8**:1–9. doi:10.1038/s41467-017-01461-z
- 838 Rosenberg AB, Roco CM, Muscat RA, Kuchina A, Sample P, Yao Z, Graybuck LT, Peeler DJ, Mukherjee S,  
839 Chen W, Pun SH, Sellers DL, Tasic B, Seelig G. 2018. Single-cell profiling of the developing mouse  
840 brain and spinal cord with split-pool barcoding. *Science* **360**:176–182.  
841 doi:10.1126/science.aam8999
- 842 Salaun C, Locatelli C, Zmuda F, González JC, Chamberlain LH. 2020. Accessory proteins of the zDHHC  
843 family of S-acylation enzymes. *Journal of Cell Science* **133**. doi:10.1242/jcs.251819
- 844 Sanders SS, Martin DDO, Butland SL, Lavallée-Adam M, Calzolari D, Kay C, Yates JR, Hayden MR. 2015.  
845 Curation of the Mammalian Palmitoylome Indicates a Pivotal Role for Palmitoylation in Diseases  
846 and Disorders of the Nervous System and Cancers. *PLoS Computational Biology* **11**:e1004405.  
847 doi:10.1371/journal.pcbi.1004405
- 848 Saunders A, Macosko EZ, Wysoker A, Goldman M, Krienen FM, de Rivera H, Bien E, Baum M, Bortolin L,  
849 Wang S, Goeva A, Nemesh J, Kamitaki N, Brumbaugh S, Kulp D, McCarroll SA. 2018. Molecular  
850 Diversity and Specializations among the Cells of the Adult Mouse Brain. *Cell* **174**:1015-1030.e16.  
851 doi:10.1016/j.cell.2018.07.028
- 852 Schneider A, Länder H, Schulz G, Wolburg H, Nave K-A, Schulz JB, Simons M. 2005. Palmitoylation is a  
853 sorting determinant for transport to the myelin membrane. *Journal of cell science* **118**:2415–23.  
854 doi:10.1242/jcs.02365
- 855 Schwarz F, Aebi M. 2011. Mechanisms and principles of N-linked protein glycosylation. *Current Opinion*  
856 *in Structural Biology* **21**:576–582. doi:10.1016/j.sbi.2011.08.005
- 857 Shimell JJ, Shah BS, Cain SM, Thouta S, Kuhlmann N, Tatarnikov I, Jovellar DB, Brigidi GS, Kass J,  
858 Milnerwood AJ, Snutch TP, Bamji SX. 2019. The X-Linked Intellectual Disability Gene *Zdhhc9* Is  
859 Essential for Dendrite Outgrowth and Inhibitory Synapse Formation. *Cell Reports* **29**:2422-2437.e8.  
860 doi:10.1016/j.celrep.2019.10.065
- 861 Shyng C, Nelvagal HR, Dearborn JT, Tyynelä J, Schmidt RE, Sands MS, Cooper JD. 2017. Synergistic effects  
862 of treating the spinal cord and brain in CLN1 disease. *Proceedings of the National Academy of*  
863 *Sciences of the United States of America* **114**:E5920–E5929. doi:10.1073/pnas.1701832114

- 864 Sjöstedt E, Zhong W, Fagerberg L, Karlsson M, Mitsios N, Adori C, Oksvold P, Edfors F, Limiszewska A,  
865 Hikmet F, Huang J, Du Y, Lin L, Dong Z, Yang L, Liu X, Jiang H, Xu X, Wang J, Yang H, Bolund L,  
866 Mardinoglu A, Zhang C, von Feilitzen K, Lindskog C, Pontén F, Luo Y, Hökfelt T, Uhlén M, Mulder J.  
867 2020. An atlas of the protein-coding genes in the human, pig, and mouse brain. *Science*  
868 **367**:eaay5947. doi:10.1126/science.aay5947
- 869 Solis GP, Valnohova J, Alvarez C, Katanaev VL. 2020. Local and substrate-specific S-palmitoylation  
870 determines subcellular localization of Gαo. *bioRxiv* 2020.08.25.266692.  
871 doi:10.1101/2020.08.25.266692
- 872 Swarthout JT, Lobo S, Farh L, Croke MR, Greentree WK, Deschenes RJ, Linder ME. 2005. DHHC9 and  
873 GCP16 constitute a human protein fatty acyltransferase with specificity for H- and N-Ras. *Journal of*  
874 *Biological Chemistry* **280**:31141–31148. doi:10.1074/jbc.M504113200
- 875 Szklarczyk D, Gable AL, Lyon D, Junge A, Wyder S, Huerta-Cepas J, Simonovic M, Doncheva NT, Morris JH,  
876 Bork P, Jensen LJ, Von Mering C. 2019. STRING v11: Protein-protein association networks with  
877 increased coverage, supporting functional discovery in genome-wide experimental datasets.  
878 *Nucleic Acids Research* **47**:D607–D613. doi:10.1093/nar/gky1131
- 879 Tasic B, Yao Z, Graybuck LT, Smith KA, Nguyen TN, Bertagnolli D, Goldy J, Garren E, Economo MN,  
880 Viswanathan S, Penn O, Bakken T, Menon V, Miller J, Fong O, Hirokawa KE, Lathia K, Rimorin C,  
881 Tieu M, Larsen R, Casper T, Barkan E, Kroll M, Parry S, Shapovalova N V., Hirschstein D, Pendergraft  
882 J, Sullivan HA, Kim TK, Szafer A, Dee N, Groblewski P, Wickersham I, Cetin A, Harris JA, Levi BP,  
883 Sunkin SM, Madisen L, Daigle TL, Looger L, Bernard A, Phillips J, Lein E, Hawrylycz M, Svoboda K,  
884 Jones AR, Koch C, Zeng H. 2018. Shared and distinct transcriptomic cell types across neocortical  
885 areas. *Nature* **563**:72–78. doi:10.1038/s41586-018-0654-5
- 886 Thomas GM, Hayashi T, Chiu SL, Chen CM, Huganir RL. 2012. Palmitoylation by DHHC5/8 Targets GRIP1  
887 to Dendritic Endosomes to Regulate AMPA-R Trafficking. *Neuron* **73**:482–496.  
888 doi:10.1016/j.neuron.2011.11.021
- 889 Thomas GM, Hayashi T, Huganir RL, Linden DJ. 2013. DHHC8-dependent PICK1 palmitoylation is required  
890 for induction of cerebellar long-term synaptic depression. *Journal of Neuroscience* **33**:15401–  
891 15407. doi:10.1523/JNEUROSCI.1283-13.2013
- 892 Tzschach A, Grasshoff U, Beck-Woedl S, Dufke C, Bauer C, Kehrer M, Evers C, Moog U, Oehl-Jaschkowitz

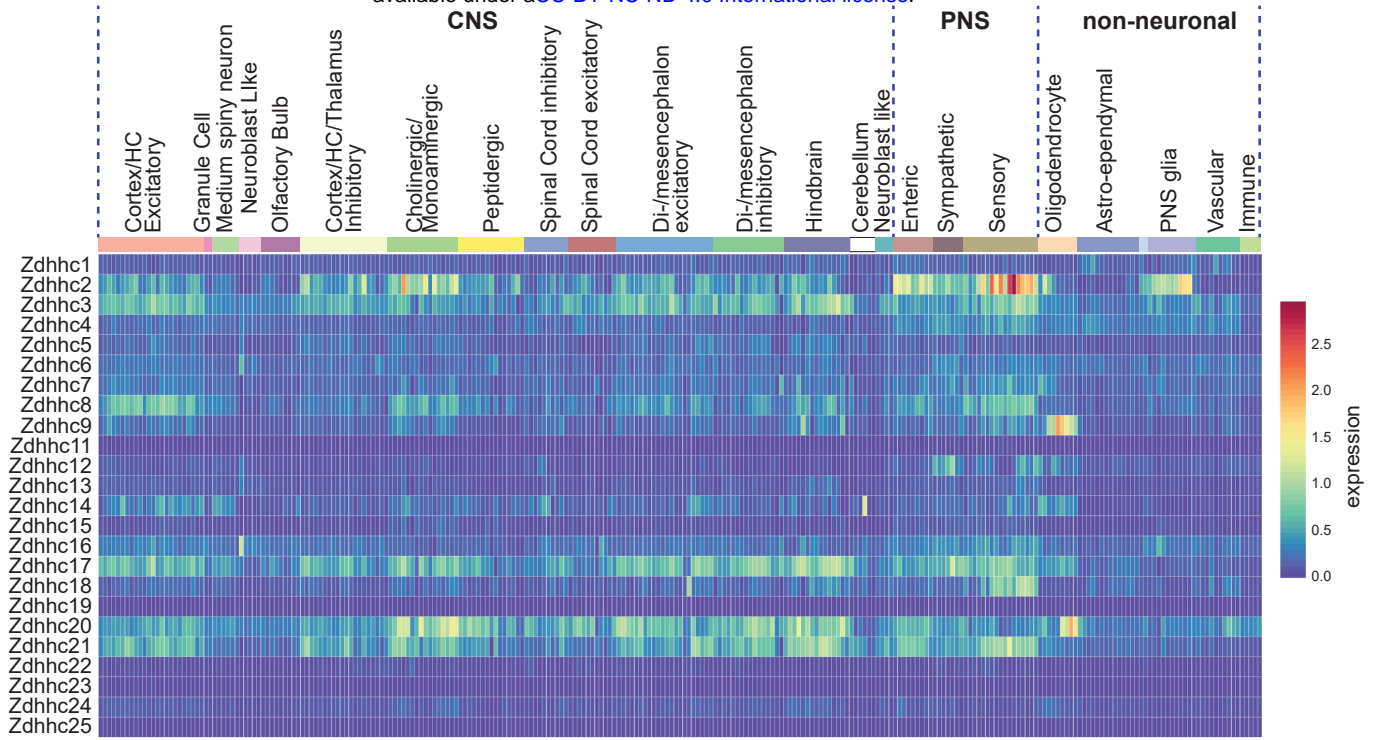
- 893 B, Donato N Di, Maiwald R, Jung C, Kuechler A, Schulz S, Meinecke P, Spranger S, Kohlhase J, Seidel  
894 J, Reif S, Rieger M, Riess A, Sturm M, Bickmann J, Schroeder C, Dufke A, Riess O, Bauer P. 2015.  
895 Next-generation sequencing in X-linked intellectual disability. *European Journal of Human Genetics*  
896 **23**:1513–1518. doi:10.1038/ejhg.2015.5
- 897 Ubersax JA, Ferrell JE. 2007. Mechanisms of specificity in protein phosphorylation. *Nature Reviews*  
898 *Molecular Cell Biology* **8**:530–541. doi:10.1038/nrm2203
- 899 Vartak N, Papke B, Grecco HE, Rossmannek L, Waldmann H, Hedberg C, Bastiaens PIH. 2014. The  
900 autodepalmitoylating activity of APT maintains the spatial organization of palmitoylated  
901 membrane proteins. *Biophysical Journal* **106**:93–105. doi:10.1016/j.bpj.2013.11.024
- 902 Verardi R, Kim JS, Ghirlando R, Banerjee A. 2017. Structural Basis for Substrate Recognition by the  
903 Ankyrin Repeat Domain of Human DHHC17 Palmitoyltransferase. *Structure* **25**:1337-1347.e6.  
904 doi:10.1016/j.str.2017.06.018
- 905 Virlogeux A, Scaramuzzino C, Lenoir S, Carpentier R, Louessard M, Genoux A, Lino P, Hinckelmann MV,  
906 Perrier AL, Humbert S, Saudou F. 2021. Increasing brain palmitoylation rescues behavior and  
907 neuropathology in Huntington disease mice. *Science Advances* **7**:799–830.  
908 doi:10.1126/sciadv.abb0799
- 909 Wagstyl K, Ronan L, Whitaker KJ, Goodyer IM, Roberts N, Crow TJ, Fletcher PC. 2016. Multiple markers  
910 of cortical morphology reveal evidence of supragranular thinning in schizophrenia. *Translational*  
911 *Psychiatry* **6**:780. doi:10.1038/tp.2016.43
- 912 Woodley KT, Collins MO. 2019. S-acylated Golga7b stabilises <sc>DHHC</sc> 5 at the plasma  
913 membrane to regulate cell adhesion. *EMBO reports* **20**:e47472. doi:10.15252/embr.201847472
- 914 Yanai A, Huang K, Kang R, Singaraja RR, Arstikaitis P, Gan L, Orban PC, Mullard A, Cowan CM, Raymond  
915 LA, Drisdell RC, Green WN, Ravikumar B, Rubinsztein DC, El-Husseini A, Hayden MR. 2006.  
916 Palmitoylation of huntingtin by HIP14 is essential for its trafficking and function. *Nature*  
917 *Neuroscience* **9**:824–831. doi:10.1038/nn1702
- 918 Yao Z, van Velthoven CTJ, Nguyen TN, Goldy J, Seden-Cortes AE, Baftizadeh F, Bertagnolli D, Casper T,  
919 Chiang M, Crichton K, Ding SL, Fong O, Garren E, Glandon A, Gouwens NW, Gray J, Graybuck LT,  
920 Hawrylycz MJ, Hirschstein D, Kroll M, Lathia K, Lee C, Levi B, McMillen D, Mok S, Pham T, Ren Q,  
921 Rimorin C, Shapovalova N, Sulc J, Sunkin SM, Tieu M, Torkelson A, Tung H, Ward K, Dee N, Smith

- 922 KA, Tasic B, Zeng H. 2021. A taxonomy of transcriptomic cell types across the isocortex and  
923 hippocampal formation. *Cell* **184**:3222-3241.e26. doi:10.1016/j.cell.2021.04.021
- 924 Yuan W, Lu L, Rao M, Huang Y, Liu CE, Liu S, Zhao Y, Liu H, Zhu J, Chao T, Wu C, Ren J, Lv L, Li W, Qi S,  
925 Liang Y, Yue S, Gao J, Zhang Z, Kong E. 2021. GFAP hyperpalmitoylation exacerbates astrogliosis and  
926 neurodegenerative pathology in PPT1-deficient mice. *Proceedings of the National Academy of  
927 Sciences of the United States of America* **118**. doi:10.1073/pnas.2022261118
- 928 Zareba-Koziol M, Bartkowiak-Kaczmarek A, Figiel I, Krzystyniak A, Wojtowicz T, Bijata M, Wlodarczyk J.  
929 2019. Stress-induced Changes in the S-palmitoylation and S-nitrosylation of Synaptic Proteins.  
930 *Molecular and Cellular Proteomics* **18**:1916–1938. doi:10.1074/mcp.RA119.001581
- 931 Zeisel A, Hochgerner H, Lönnerberg P, Johnsson A, Memic F, van der Zwan J, Häring M, Braun E, Borm LE,  
932 La Manno G, Codeluppi S, Furlan A, Lee K, Skene N, Harris KD, Hjerling-Leffler J, Arenas E, Ernfors P,  
933 Marklund U, Linnarsson S. 2018. Molecular Architecture of the Mouse Nervous System. *Cell*  
934 **174**:999-1014.e22. doi:10.1016/j.cell.2018.06.021
- 935 Zeisel A, Moz-Manchado AB, Codeluppi S, Lönnerberg P, Manno G La, Juréus A, Marques S, Munguba H,  
936 He L, Betsholtz C, Rolny C, Castelo-Branco G, Hjerling-Leffler J, Linnarsson S. 2015. Cell types in the  
937 mouse cortex and hippocampus revealed by single-cell RNA-seq. *Science* **347**:1138–1142.  
938 doi:10.1126/science.aaa1934
- 939

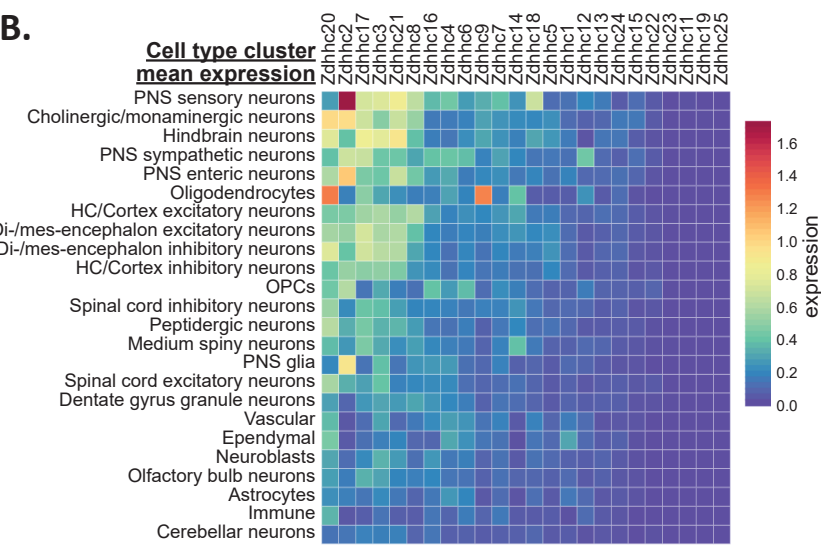


**Figure 1**

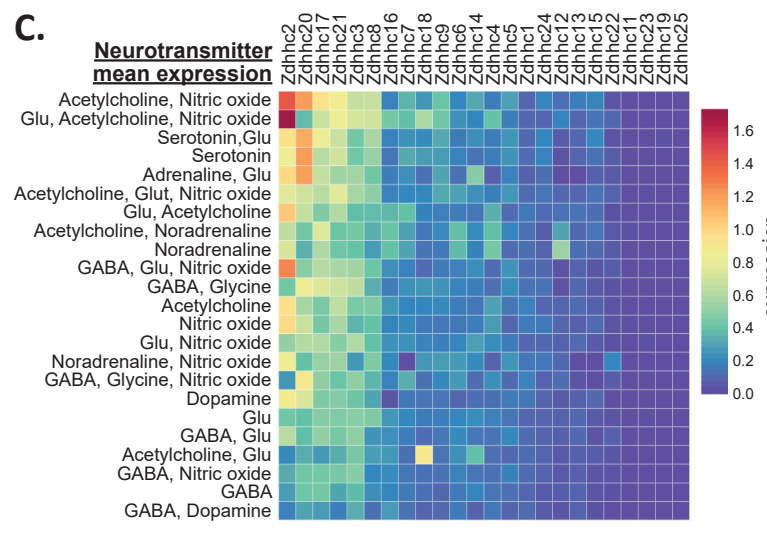
**A.**



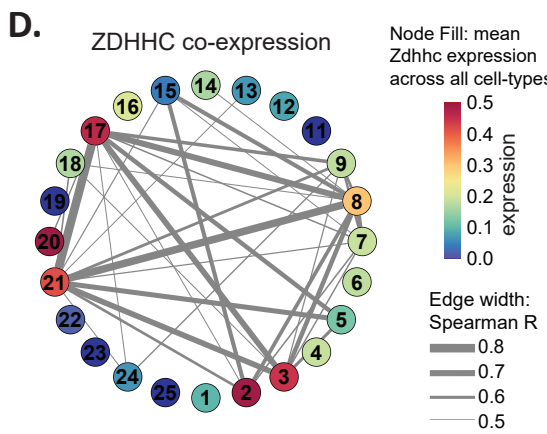
**B.**



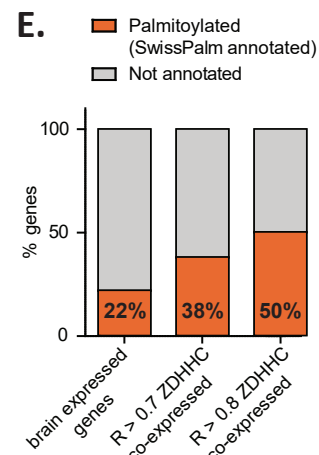
**C.**



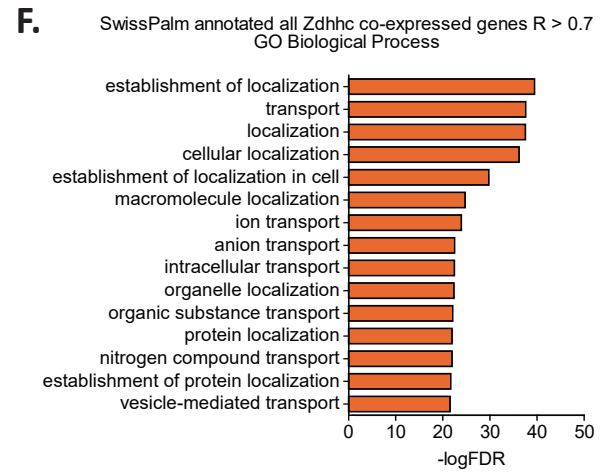
**D.**

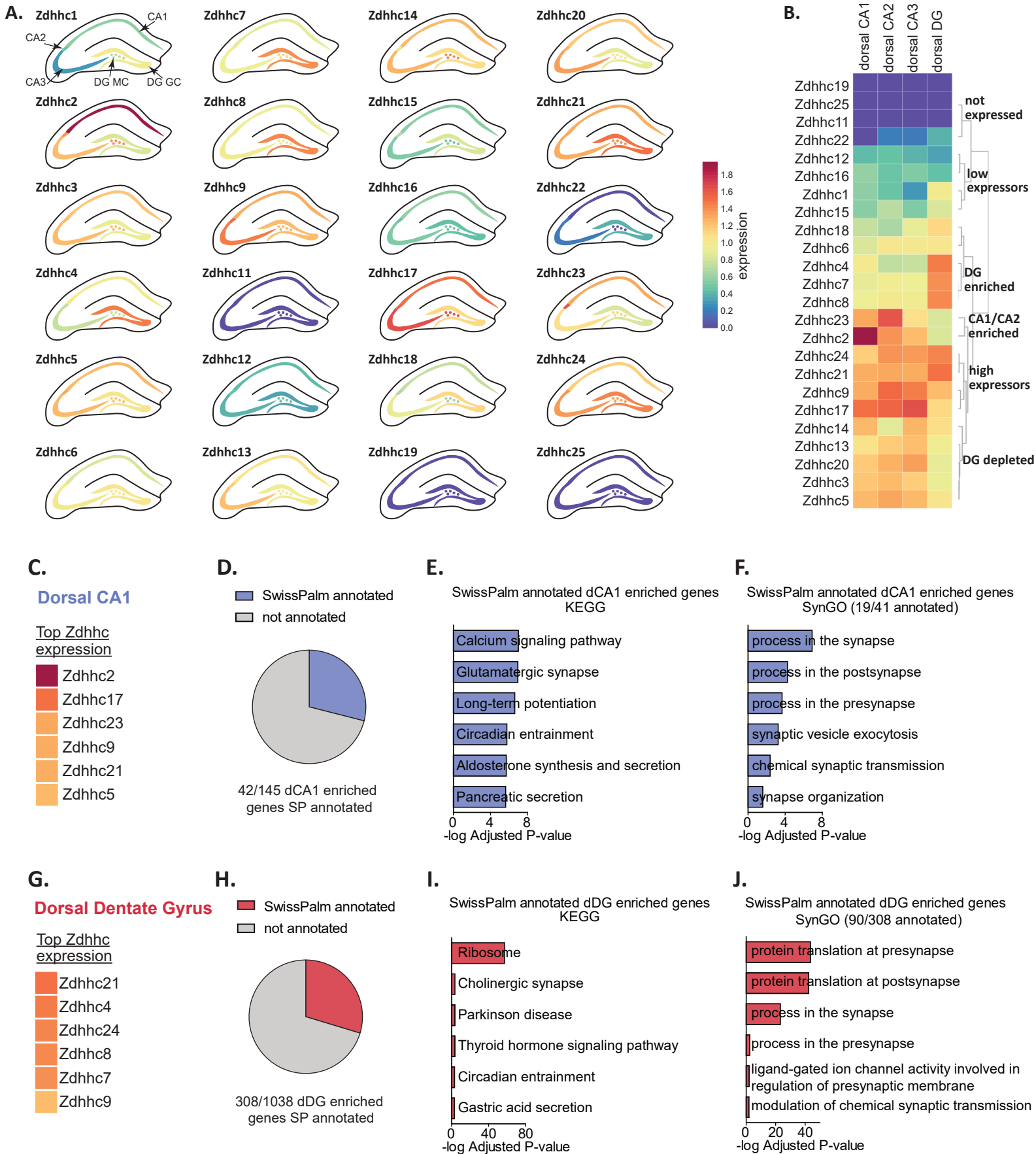


**E.**

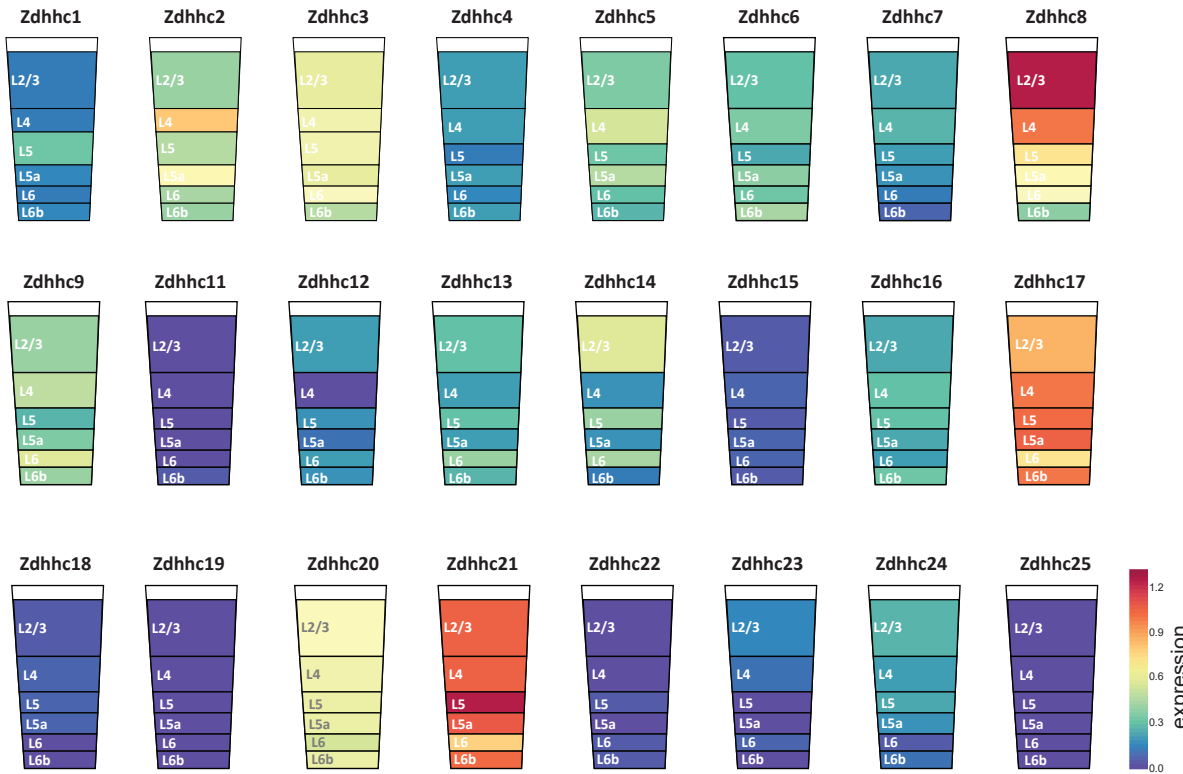


**F.**





A.

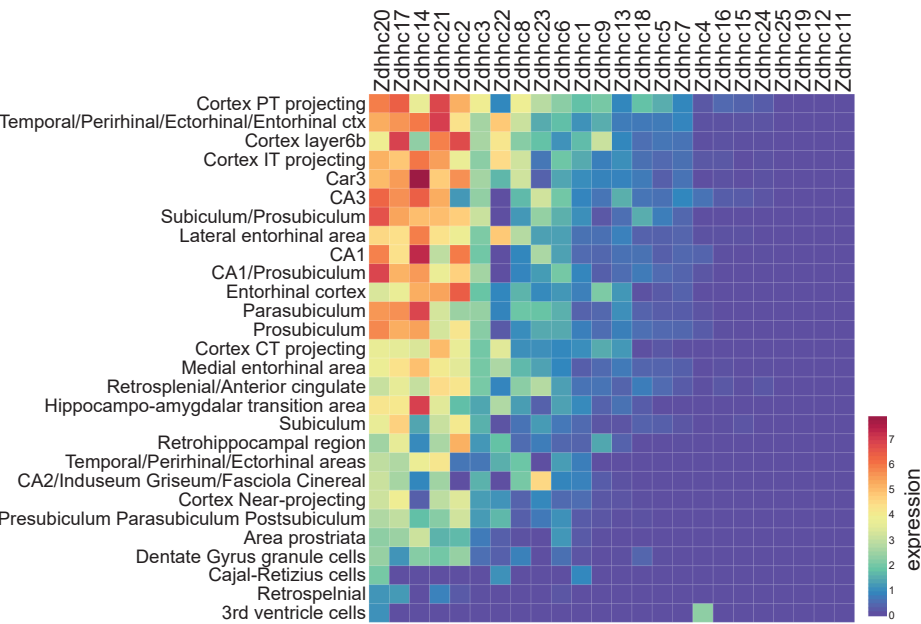


B.



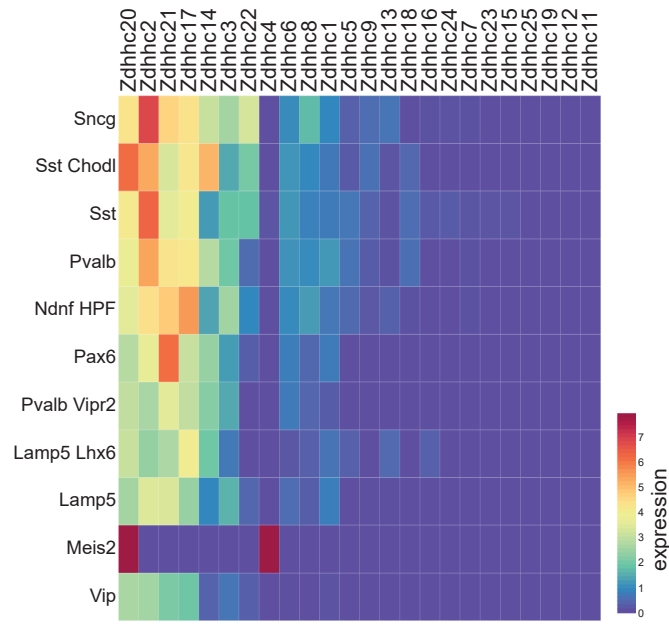
C.

Allen Brain 10X glutamatergic neurons



D.

Allen Brain 10X GABAergic neurons



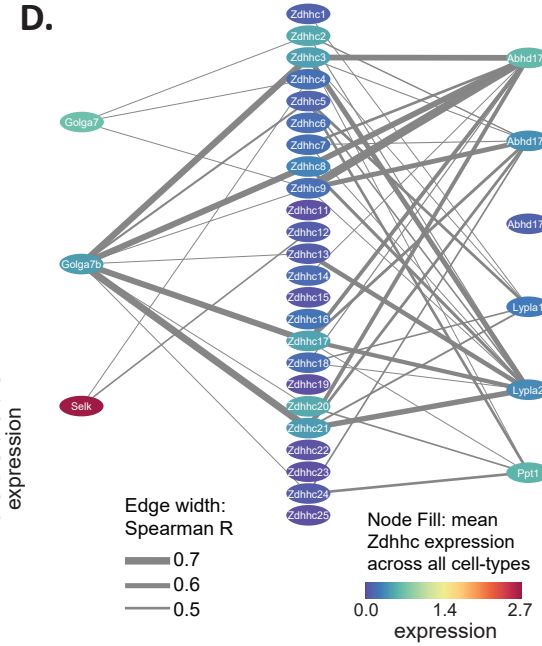
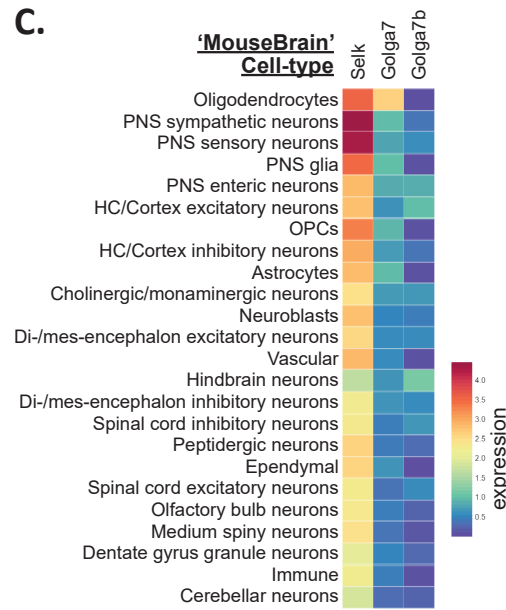
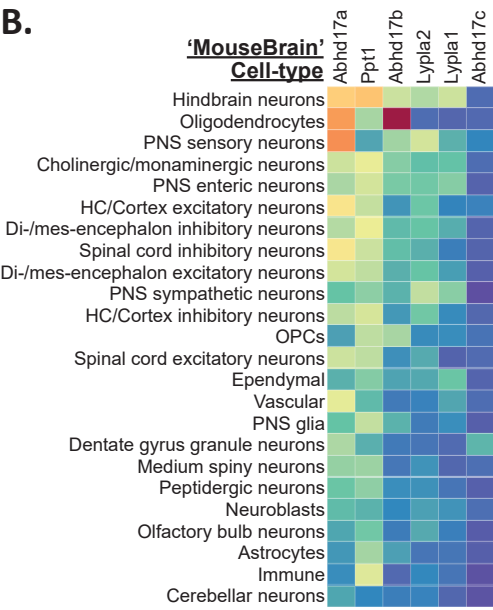
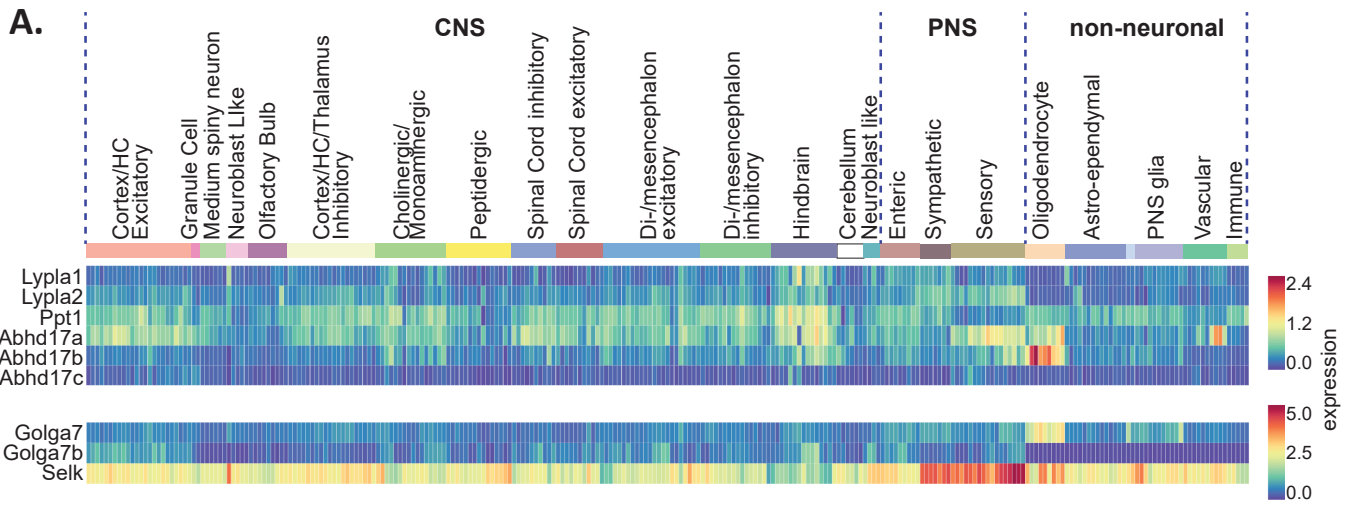
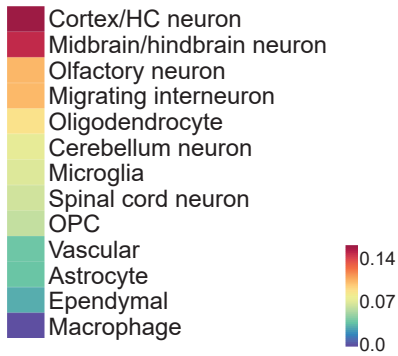
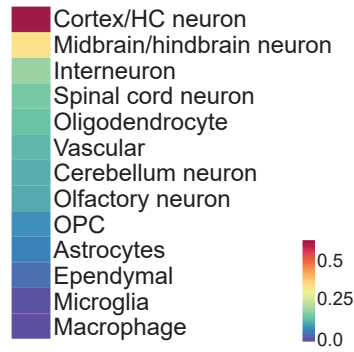


Figure 5

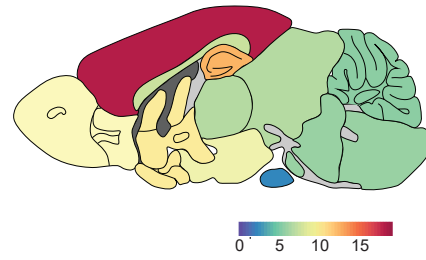
**A. *Zdhhc8* neonatal expression  
Rosenberg et al <P11**



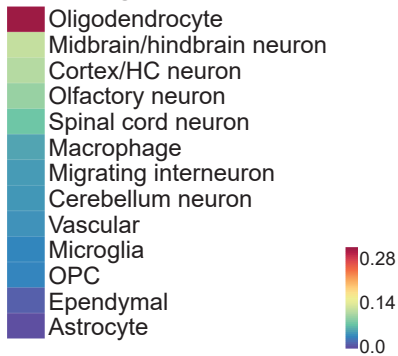
**B. *Zdhhc8* adolescent expression  
'MouseBrain' P25**



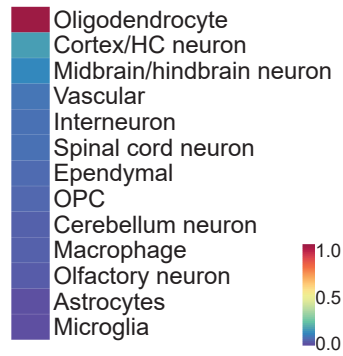
**C. *Zdhhc8* adult expression  
'Protein Atlas' Mouse P60**



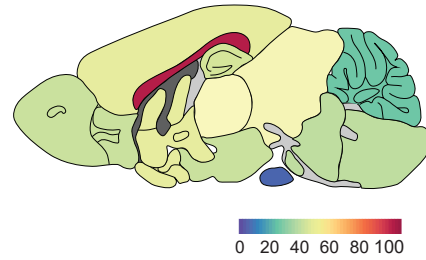
**D. *Zdhhc9* neonatal expression  
Rosenberg et al <P11**



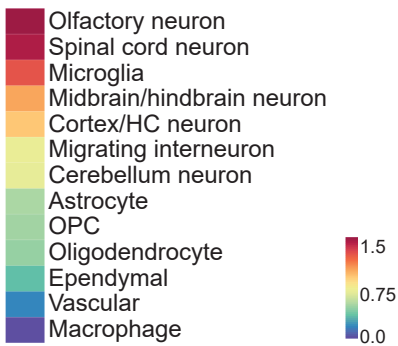
**E. *Zdhhc9* adolescent expression  
'MouseBrain' P25**



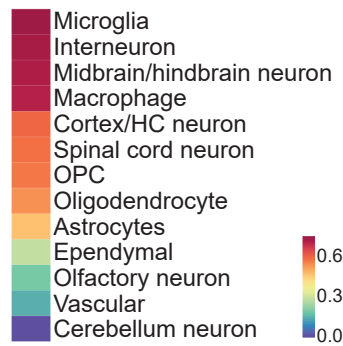
**F. *Zdhhc9* adult expression  
'Protein Atlas' Mouse P60**



**G. *Ppt1* neonatal expression  
Rosenberg et al <P11**



**H. *Ppt1* adolescent expression  
'MouseBrain' P25**



**I. *Ppt1* adult expression  
'Protein Atlas' Mouse P60**

